HER2 missense mutations have distinct effects on oncogenic signaling and migration

by

Daniel J. Zabransky

A dissertation submitted to the Johns Hopkins University in conformity with the requirements for the degree of Doctor of Philosophy

Baltimore, Maryland

July 2015

Abstract

Recurrent *HER2* missense mutations have been reported in human cancers. These mutations occur primarily in the absence of *HER2* gene amplification such that most *HER2* mutant tumors are classified as “negative” by FISH or immunohistochemistry assays. It remains unclear whether non-amplified *HER2* missense mutations are oncogenic, and whether they are targets for HER2-directed therapies that are currently approved for the treatment of *HER2* gene-amplified breast cancers. Here we functionally characterize *HER2* kinase and extracellular domain mutations through gene editing of the endogenous loci in *HER2* non-amplified human breast epithelial cells. In *in vitro* and *in vivo* assays, the majority of *HER2* missense mutations do not impart detectable oncogenic changes. However, the *HER2* V777L mutation increased biochemical pathway activation and, in the context of a *PIK3CA* mutation, enhanced migratory features *in vitro*. However, the V777L mutation did not alter *in vivo* tumorigenicity or sensitivity to HER2-directed therapies in proliferation assays. Our results suggest the oncogenicity and potential targeting of *HER2* missense mutations should be considered in the context of cooperating genetic alterations and provide new insights into functional analysis of *HER2* mutations and strategies to target them.

Thesis Advisor: Ben Ho Park MD, PhD

Thesis Readers: Ben Ho Park MD, PhD

Paula Hurley, PhD

Acknowledgements

I am extremely fortunate to have been surrounded by incredible people leading up to and throughout my time in graduate school. I owe my deepest thanks and appreciation to many people, but there are a few I would like to acknowledge here.

First, I would like to thank my thesis advisor, Dr. Ben Ho Park. You are a brilliant scientist, a fantastic mentor, and the best role model a trainee could have. It is impossible to keep track of all the times where your enthusiasm and encouragement have helped me get through the challenges I have faced in my work. You were always there with great advice, an anecdote from your own training, or a lame (but sometimes funny) joke when I needed a bit of perspective or reassurance. In addition to your qualities as a scientist, you are also one of the most fun-loving people I know. It is your attitude and personality that enables the Park Lab to be the exciting, amusing, and occasionally absurd place to work that it is. There are very few people like you, and I consider myself extremely lucky to have learned from you.

I would next like to thank all the past and present members of the Park Lab. My fellow lab members have always been willing to help each other in any way possible, and I feel fortunate to have spent these years surrounded by smart, talented people like them. I would also like to thank Dr. Josh Lauring for his insight, suggestions, and for commiserating with me in the tissue culture room. It was a privilege to have another incredible scientist to work with and learn from during my time in the lab.

My family deserves more acknowledgement and thanks than I could ever give them. To my dad, my mom, and my brother, thank you for all that you do for me and for

always supporting me. Mom and Dad, without you I would not have had the opportunity to go to medical and graduate school. When I look back at my childhood, I recognize all the choices and sacrifices you made to help me succeed, and I appreciate what amazing parents you are. You have always pushed me to do my best and guided me when I needed it the most. There was never a second where I didn't feel like you were helping me accomplish my goals. Thank you for always being there for me.

Finally, and most importantly, I would like to thank my wife, Caitlin. Your support and love have always been unconditional, and there is no way I could make it through this process without you. It is amazing to think that has been six years since you followed me to Baltimore to start our life together. Thank you for all that you do and all that you have sacrificed so that we can both pursue our dreams. We have grown so much together, and I cherish every day that I have with you. It is inspiring to see how dedicated and hard-working you are in everything you do in your life. You are an amazing person who makes a positive impact on the lives of everyone around you. I am so proud to have you as my best friend and partner in life. I love you.

Table of Contents

List of Tables

List of Figures

1 Introduction

Breast cancer overview

Breast cancer is the most commonly diagnosed cancer in women in the United States. There are approximately 232,000 new cases diagnosed and nearly 40,000 deaths each year, making breast cancer the second most common cause of cancer related deaths among women in the United States (1). The development of breast cancer is multi-faceted and complex, involving predisposing inherited genetic alterations, carcinogenic environmental exposures, and many other factors, but a major cause of breast carcinogenesis is the accumulation of and selection for tumor-promoting somatic genetic alterations. Genetic alterations, including mutations, rearrangements, deletions, and amplifications, of certain genes allow normal cells to undergo transformation into cancer cells and drive the growth and survival of a tumor (2).

Across breast cancers, the majority of mutations occur at low frequencies (i.e. a given mutation occurs in a low percentage of diagnosed breast cancers), with only a few genes, including *PIK3CA* and *TP53*, occurring at relatively higher frequencies (3-5). However, the high incidence of breast cancer makes the study of low frequency mutations potentially impactful for tens of thousands of patients each year. Cancer cells often rely on the action of mutated oncogenes for growth and survival, making oncogenes an extremely important and promising target for cancer therapies (6). Characterization of mutations in oncogenes found in breast cancer can provide understanding into the mechanisms through which these mutations promote the initiation, growth, and survival of cancer cells. Insights into how oncogenic mutations drive cancers have led to the development of more effective and less toxic anti-cancer therapies that shut down the molecular pathways cancers use to grow and survive (7,8).

Recent cancer genome sequencing studies have demonstrated that somatic point mutations in the gene *HER2* occur in a number of cancers, including 2-4% of breast cancers (9-12). While there has been extensive work showing that amplification/overexpression of *HER2* can deregulate normal signaling pathways and promote the formation and growth of malignant tumors, the functional consequences of *HER2* missense mutations remains relatively unstudied. *HER2* mutations cluster in the extracellular and kinase domains of *HER2* and are found at high clonal frequencies in patient tumors, indicating that they may be driving tumor formation or growth, thus presenting a potential new target for anti-cancer therapies.

HER2 background and function

Discovery of HER2

The receptor tyrosine kinase HER2 (encoded by the gene *HER2*/*ErbB2*) has been a focus of cancer research since its discovery in the 1980s. The first work leading to the discovery of *HER2* utilized a calcium-phosphate DNA precipitation technique to introduce DNA from rat neuro/glioblastoma cells into NIH3T3 mouse fibroblasts (13,14). The introduction of this DNA resulted in morphological changes in NIH3T3 cells and promoted a transformed phenotype. In 1984, cells were transformed by the introduction of mutant rat DNA derived from carcinogen-induced neuroblastomas (15); the oncogene responsible for this transformation was the same as previously identified by Shih *et al*. and was given the name *neu*. *Neu* was later shown to encode a 185 kDa phosphoprotein that had extensive homology to the kinase domain of the epidermal growth factor receptor (EGFR/ErbB1) (16). Further work mapped a human ortholog to *neu*, *HER2*, to chromosome 17, distinct from *EGFR* on chromosome 7 (17).

HER2 gene and protein structure

The *HER2* gene is located on chromosome 17q12 and contains 30 exons, 26 of which are coding exons. The predominate *HER2* mRNA transcript variant encodes a 185 kDa receptor tyrosine kinase protein comprised of 1,255 amino acids. HER2 is a member of the ErbB family of transmembrane receptor tyrosine kinases which includes the epidermal growth factor receptor (EGFR/ErbB1), HER3 (ErbB3), and HER4 (ErbB4) (18). These receptors are each comprised of

five domains including an extracellular domain, a transmembrane domain, a juxtamembrane region, a tyrosine kinase domain, and a C-terminal regulatory region (7,19,20). The extracellular domain of ErbB receptors are further divided into four distinct sub-domains. Typically, sub-domains II and IV interact until the receptor binds ligand. After ligand is bound, sub-domains I and III are brought close together, which breaks the interaction between sub-domains II and IV, allowing sub-domain II to freely facilitate receptor dimerization and initiate signal transduction (21). In contrast to other ErbB receptors, HER2 is considered an orphan receptor that does not bind a specific ligand. However, HER2 always exists in a ligand-activated conformation where extracellular sub-domain II is available for receptor dimerization (22). This property makes HER2 the preferred dimerization partner for other ligand bound ErbB receptor family members (20,23).

The intracellular tyrosine kinase domains of HER2 and other ErbB receptors are comprised of docking sites for adapter proteins that promote downstream signaling. Ligand binding and receptor dimerization acts as an allosteric activator of kinase domain catalytic activity which leads to the phosphorylation of tyrosine residues in the kinase domain (24). Interestingly, HER3 lacks certain key residues thought to be required for catalytic activity in the kinase domain, and recent studies have shown the catalytic activity of HER3 to be roughly 1,000 fold less than that of EGFR (24,25). Due to this low catalytic activity, HER3 is thought to function primarily as an allosteric activator in

asymmetric dimers with other ErbB receptors. In contrast, HER2 has the most potent tyrosine kinase activity of the ErbB receptors (8).

HER2 mediated signaling

ErbB receptors are activated by ligands including epidermal growth factor (EGF), neuregulins, and transforming growth factor-α (TGF-α) among others. Upon ligand binding, ErbB receptors undergo a conformational rearrangement from a closed/tethered state to an open/extended conformation which exposes regions necessary for receptor dimerization. This promotes homodimerization and heterodimerization of the receptors. While HER2 cannot directly bind ligands, it is preferentially recruited as a partner in heterodimers when these ligands are bound to other ErbB family members, due to the fact that HER2 always exists in an open/extended, active conformation.

Unique patterns of C-terminal autophosphorylation then induce and dictate specific interactions with cytoplasmic signal transduction partners, including GRB2, Src, Shc, and p85, specific to each ErbB receptor. These events then in turn promote a wide variety of cellular processes including, but not limited to, proliferation, motility, and escape from apoptosis. HER2's unique ability to dimerize without ligand binding allows it to cause signaling pathway dysregulation when *HER2* is amplified/overexpressed.

The main downstream signaling pathways activated by HER2 and ErbB receptors are the MAP Kinase and the PI3K/AKT pathways. The MAP Kinase pathway is activated by ErbB receptors when the GRB2 adapter protein is

recruited directly to phosphorylated C-terminal tyrosine sites or indirectly by binding Src homology 2-containing (Shc). GRB2-Son of sevenless (Sos) complexes form and recruit Ras, leading to signal transduction through the rest of the MAP Kinase pathway to promote cellular proliferation, angiogenesis, differentiation, and migration.

ErbB receptors can activate the PI3K/AKT pathway through direct recruitment of the p85 regulatory subunit of PI3K to phosphorylated tyrosine residues, which leads to activation of the p110α catalytic subunit of PI3K. Additionally, GRB2 can interact with ErbB receptors and activate Ras, which then activates p110α mediated signaling. Once activated, PI3K phosphorylated phosphatidylinositol 4,5-bisphosphate (PIP2) to phosphatidylinositol 3,4,5-trisphophate (PIP3). PIP3 in turn binds to the pleckstrin homology domain of AKT. Then, phosphatidylinositol-dependent kinase 1 (PDK1) phosphorylates and activates AKT. Activated AKT phosphorylates many downstream signaling proteins associated with cellular survival, growth, proliferation, and angiogenesis. HER2/HER3 dimers are the most potent activators of PI3K/AKT signaling. This is due to the strong tyrosine kinase activity of HER2, while HER3 has 6 p85 binding sites in its kinase domain to promote PI3K/Akt pathway activation (20). In addition to the MAP Kinase and PI3K/Akt pathways, ErbB receptors can also activate JAK/STAT, Src, and WNT signaling pathways (7,20).

Clinical importance of *HER2* in breast cancer

In addition to their key role in normal cellular growth and maintenance, the dysregulation of ErbB receptors has been extensively implicated in the

development of numerous cancers. In a landmark study, Slamon *et al.* found that *HER2* is amplified in over 20% of breast cancers (26). HER2 is overexpressed in the majority of cases of gene amplification and can also be overexpressed in the absence of clear *HER2* amplification. *HER2* amplification/overexpression is associated with decreased survival and time to relapse in breast cancer. It has also been demonstrated that the growth of *HER2*-amplified/overexpressed primary breast tumors as well as pulmonary metastases require the continuous expression of HER2 to drive tumor growth (27). In addition to breast cancer, *HER2* amplification and overexpression has been described in other cancer types, including ovarian, gastric, endometrial and lung cancer, where it is also an indicator of poor prognosis (7,8,20).

With the identification of HER2 as a major driver in breast and other cancers, it has become a prime target in the development of cancer therapies. Two major classes of drugs targeting HER2, antibodies and tyrosine kinase inhibitor, are currently in clinical use for the treatment of *HER2*-amplified/overexpressed cancers. Antibodies, including the humanized monoclonal antibody trastuzumab, can bind to the extracellular domain of HER2 and downregulate HER2 signaling through a complex variety of mechanisms. For example, trastuzumab can inhibit receptor homo or heterodimerization, remove HER2 receptors from the cell surface through endocytic internalization and degradation, and promote an immunological response against the tumor cells by activating a process known as antibody-dependent cellular cytotoxicity (ADCC) when bound to a tumor cell (19,20).

A number of small molecule inhibitors targeting HER2 are FDA approved or in development. These include lapatinib, an EGFR/HER2 targeted reversible tyrosine kinase inhibitor which competitively binds to the ATP-binding pocket of the receptor kinase domain and neratinib, which is an irreversible dual EGFR/HER2 inhibitor (20). These small molecules potently disrupt HER2 signaling, leading to inhibition of the MAP Kinase and PI3K/AKT pathways. Interestingly, lapatinib has been shown to provide a clinical benefit in patients with *HER2*-amplified/overexpressed cancers that have progressed after treatment with trastuzumab (28). The successful use of these targeted therapies in cancer patients has further demonstrated the importance of targeting HER2 as a driver of tumorigenesis, however, many patients quickly develop resistance to HER2 targeted therapies through a variety of mechanisms, including activating mutations in the PI3K/AKT and MAP Kinase pathways (8,19,20).

Identification of *HER2* missense mutations in human cancers

Large scale cancer genome sequencing efforts have provided a way to identify low frequency mutations that may play important roles in the development of cancer. A number of these studies have found recurrent mutations in *HER2* in human cancers including breast, stomach, bladder, and lung cancers (10,11,29). In breast cancer, these mutations are most often found in patients as single copies without amplification/overexpression of *HER2* (HER2-"negative" breast cancers) though HER2 protein expression is often still present in these tumors. While other methods of mutational activation, including kinase domain insertions and deletions of the extracellular domain, have been described

to activate HER2, the diversity and low frequencies of individual somatic missense mutations have made it more difficult to fully characterize their potential oncogenic effects (19).

Prior studies of *HER2* missense mutations have utilized overexpression of mutant *HER2* cDNAs to investigate the effects of *HER2* missense mutations in human cells. These studies have implicated a number of these mutations as potently activating and oncogenic (10,12,30-32). Notably, the V777L kinase domain mutation was described to increase HER2 kinase activity, activate MAP Kinase signaling, and increase invasiveness in three-dimensional culture, anchorage independent growth in soft agar, and tumor growth as xenografts *in vivo* when overexpressed in MCF-10A and MCF7 cells. The HER2 targeted drugs lapatinib and neratinib inhibited the signaling and transformed phenotypes imparted by the V777L mutation. Other missense mutations, including the extracellular domain mutations G309A and S310F increase reduction sensitive covalent dimerization and receptor activation when overexpressed. The G309A and S310F mutations also increased features of transformation and were found to respond to treatment with trastuzumab in overexpression studies (10,30). Additionally, one missense mutation, L755S, has been associated with biochemical signaling and proliferative resistance to lapatinib when overexpressed, potentially due to steric interference of the binding site for small molecule kinase inhibitors (10,33,34).

Single copy knock in models in the study of mutant oncogenes

Past studies comparing overexpression of a mutant cDNA to single nucleotide knock in of mutant oncogenes have shown dramatic differences in signaling and transformed phenotypes (35-37). In one example, knock in of the mutant EGFR delE746-A750 allele into MCF-10A cells recapitulated biochemical signaling phenotypes seen in overexpression models, but did not promote the transformed phenotype of anchorage independent colony formation in soft agar in MCF-10A cells that occurred with overexpression (37). Furthermore, differences in phenotypes between overexpression and single copy knock in models of mutant oncogenes have been reported in the study of genes including *AKT1* and *KRAS* (35,36).

In addition to recapitulating endogenous expression levels, another important example to consider in modeling mutant oncogenes in the genetic context in which these mutations exist. For example, it was shown that *KRAS* G12V mutations as single copies have relatively little effect in breast epithelial cells, but have a profound effect on cancerous phenotypes and tumorigenicity when coupled with a *PIK3CA* oncogenic hotspot mutation (38). Given these caveats to the overexpression of mutant oncogenes, we used two HER2 non-amplified human breast epithelial cell lines to create an isogenic panel of *HER2* missense knock in mutants. To our knowledge, this represents the first study of the effects of single copy *HER2* mutations under endogenous gene expression levels comparable to what has been observed in *HER2*-mutant cancers without *HER2*-amplification/overexpression.

2 Methods

Cell culture:

The non-transformed human epithelial cell line MCF-10A and its derivatives were maintained in DMEM/F12 (1:1) supplemented with 5% horse serum (Life Technologies, Carlsbad, CA), 20 ng/ml EGF (Sigma-Aldrich, St. Louis, MO), 10 µg/ml insulin (Life Technologies), 0.5 µg/ml hydrocortisone (Sigma-Aldrich), and 0.1 µg/ml cholera toxin (Sigma-Aldrich), and 1% Penicillin-Streptomycin (Life Technologies). MCF-10A cell lines with a *PIK3CA* E545K mutation were maintained in this same media without EGF supplementation. For assays using MCF-10A and its derivatives, DMEM:F12 (1:1) media containing 1% charcoal dextran stripped FBS (Life Technologies) with insulin, hydrocortisone, cholera toxin and without EGF, with 0.2ng/mL, or with 20ng/mL EGF, was used as indicated.

The MCF7 cell line and its derivatives were maintained in DMEM media with 5% fetal bovine serum (Life Technologies) and 1% Penicillin-Streptomycin (Life Technologies). For assays with MCF7 and its derivatives, DMEM:F12 (1:1) media without phenol red was supplemented with 0.5% charcoal dextran stripped FBS (serum starved) or DMEM media with 5% FBS (serum supplemented) was used as indicated unless otherwise noted. MCF-10A parental, MCF7 parental, and HEK-293T cells were purchased from ATCC (Manassas, VA). MCF-10A + E545K cells were derived in a previous study (39). The MCF7 corrected cell line was also generated in a previous study (40). MCF-10A *HER2* wild type, G309A, L755S, and V777L overexpression cell lines were generated in a previous study (10). Parental cell lines were authenticated via short tandem repeat profiling analysis at the Johns Hopkins Genetic Resources Core Facility. A complete list of cell lines generated and used in this study can be found in Table 1.

Gene targeting and generation of *HER2* missense mutation cell lines:

Gene targeting was carried out using recombinant AAV vectors as previously described (39). Gene targeting of *HER2* was carried out using one of three distinct recombinant AAV vectors (Figure 1A). Gene targeting was performed as previously described (Figure 1B) (41). AAV vectors were produced by ligating wild type homology arms generated by PCR into an AAV plasmid backbone (Agilent, La Jolla, CA). Site-directed mutagenesis by overlap extension PCR with subsequent cloning into the parental AAV plasmid backbone was used to generate a targeting construct for each *HER2* mutation that was studied (42). Infectious virus was prepared by co-transfecting HEK-293T cells with pHelper,

pRC (Agilent) and the respective *HER2* mutation carrying rAAV targeting plasmid. Approximately 10^6 cells were used for each viral infection, and a sib selection strategy was employed as previously described (43). Targeted neomycin resistant clones were isolated and cells were then exposed to Cre-expressing recombinant adenovirus to remove the neomycin cassette as previously described (41). All clones were subjected to confirmation by Sanger sequencing of genomic DNA and cDNA to ensure each clone harbored the intended *HER2* mutation as single expressed copies (Figure 2). Single-stranded cDNA was generated using First Strand cDNA Synthesis Kit (Amersham Biosciences, Piscataway, NJ). At least two clones were isolated for each mutation in each parental background. In addition, AAV gene targeting using wild type *HER2* constructs to create targeted wild type controls for each locus. Primer sequences for homology arm construction, mutagenesis, pre-Cre PCR screening, post-Cre PCR screening, genomic DNA sequencing, and cDNA sequencing can be found in Table 2 and Table 3.

Overexpression of *HER2*, *HER3*, and *PIK3CA* cDNAs in human cells:

HEK-293T cells were transfected using the Fugene 6 system (Promega, Fitchburg, WI). pCFG5 plasmids containing wild type, G309A, L755S, or V777L *HER2* cDNAs, and LXSN plasmids containing wild type or E545K mutant *PIK3CA* were derived in previous studies (10,38). A wild type *HER3* expression vector was created by subcloning *HER3* cDNA from the pCMV6-XL4-ERBB3 plasmid (SC118918; Origene, Rockville, MD) into a pIRES-neo3 backbone.

Lysates from HEK-293T cells harvested approximately 48 hours after transfection with the indicated plasmids.

Cell proliferation assays:

Exponentially growing cells were washed twice with HBSS and seeded in the indicated media. Cells were seeded at a density of $2x10^4$ cells per well of a 6-well tissue culture dish on day 0. Medium was changed every third day. Cells were harvested on the indicated days and were counted using a Beckman Coulter counter and relative proliferation was calculated using the average proliferation of the first time point for each cell line as a reference. Results for targeted wild type and *HER2* mutant cell lines represent data from two or more clones unless otherwise indicated. For some assays, cells were also fixed and stained with 3.7% formaldehyde containing 0.2% crystal violet (Sigma-Aldrich).

Drug inhibitor assays:

Lapatinib, neratinib, and BYL-719 were obtained from Selleck (Houston, TX) and were dissolved in dimethyl sulfoxide (DMSO). Trastuzumab was obtained from the Johns Hopkins Research Pharmacy (Baltimore, MD) and was dissolved in bacteriostatic water. $1\text{-}2x10^3$ cells per well were plated into 96-well plates on day 0. MCF-10A derivatives were grown in assay media containing 20ng/μL EGF, MCF-10A derivatives with *PIK3CA* E545K mutation were grown in assay media without EGF, while MCF7 and MCF7 corrected derivatives were grown in assay media containing 5% FBS. On day 1, media was changed to contain the indicated concentration of drug or appropriate vehicle control. Alamar

blue (Life Technologies) was used to determine cell proliferation on day 6 according to the manufacturer's instructions. IC_{50} values were calculated using the log(inhibitor) vs. response – variable slope (four parameters) nonlinear regression function in Graphpad Prism 5 (GraphPad Software, La Jolla, CA). Experiments were performed in sextuplet for each concentration of drug for each cell line.

Colony formation assay in semisolid medium:

$5x10^3$ exponentially growing cells were cast in 3 mL of top-later medium comprised of assay media with 20ng/mL EGF for MCF-10A derivatives or 5% FBS for MCF7 derivatives and 0.4% UltraPure Agarose (Life Technologies) poured on top of a 2mL bottom layer containing 0.6% agarose in 6-well tissue culture plates. Media was refreshed once a week. For assays with inhibitors or DMSO vehicle controls (0.5%), compounds were added at the indicated concentrations the day after plating. After 4 weeks of incubation, the colonies were stained with crystal violet and visually inspected for proliferating colonies. One to three fields per well were counted to for each well per experiment with wells plated in at least duplicate. Photographs were taken with a Nikon SMZ 1500 stereoscopic zoom microscope.

Acinar morphogenesis assay:

Morphogenesis assays were conducted in growth factor reduced Matrigel (BD Biosciences, San Jose, CA) as previously described (44). For acinar morphogenesis assays in the presence of inhibitors or DMSO vehicle controls

(0.5%), compounds were added at the indicated and media was changed every four days. Photographs were taken under phase contrast microscopy (Nikon) after 12 days of incubation.

Immunoblotting:

Cells were washed twice and seeded in the indicated media. After 48 hours, cells were harvested for protein lysates, and immunoblotting was conducted as previously described (35). Briefly, whole-cell protein extracts prepared in Laemmli sample buffer were resolved by SDS-Page using NuPAGE gels (Invitrogen), transferred to polyvinylidene diflouride (PVDF) membranes (Invitrogen), and probed with primary antibody followed by incubation with horseradish peroxidase-conjugated secondary antibodies. The primary antibodies used in this study include anti-phospho ErbB-2/HER-2 (Tyr1248) rabbit antibody (06-229; Millipore, Billerica, MA), anti-HER2/ErbB2 rabbit antibody (2242; Cell Signaling Technology, Danvers, MA), anti-phospho-p44/p42 MAP kinase (Thr 202/Tyr 204) rabbit antibody (4370; Cell Signaling Technology), anti-p44/p42 MAP kinase rabbit antibody (9102; Cell Signaling Technology), anti-phospho-EGF receptor (Tyr 1068) rabbit antibody (3777; Cell Signaling Technology), anti-EGF receptor rabbit antibody (4267; Cell Signaling Technology), anti-phospho AKT (Ser 473) rabbit antibody (9271; Cell Signaling Technology), anti-AKT rabbit antibody (9272; Cell Signaling Technology), anti-phospho p90RSK rabbit antibody (9341; Cell Signaling Technology), anti-p90RSK rabbit antibody (9333; Cell Signaling Technology), anti-phospho HER3/ErbB3 (Tyr 1289) rabbit antibody (4791; Cell Signaling Technology), anti-

HER3/ErbB3 rabbit antibody (4754; Cell Signaling Technology), anti-PI3 Kinase p85 (19H8) (4257; Cell Signaling Technology), anti-phospho p70 S6 Kinase (Thr389) (9205; Cell Signaling Technology), anti-p70 S6 Kinase (9202; Cell Signaling Technology), and anti-GAPDH rabbit antibody (5174; Cell Signaling Technology).

Immunoprecipitation:

Cells were grown in serum starved media conditions and were then washed with ice-cold PBS, scraped, and lysed on ice in lysis buffer containing 1% Triton X-100, 10% glycerol, 100mM NaCl, 50mM Hepes (pH 7.2), 10mM NaF (all from Sigma-Aldrich), 10mM Na_3VO_4 (New England Biosciences, Ipswich, MA), and Roche minitab cOmplete protease inhibitor with EDTA (Roche, Basel, Switzerland). Lysates were cleared by centrifugation at 14,000 rpm for ten minutes at 4°C. Protein concentration was measured using the BCA protein assay reagent (Pierce, Rockford, IL). Immunoprecipitation was performed by incubating 1mg of protein extract with 1µg of anti-HER3 antibody (Millipore 05-390) overnight at 4°C. Lysates were then incubated with Dynabeads Protein G for immunoprecipitation (Life Technologies) for 4 hours at 4°C. Beads were then washed with lysis buffer and boiled for 5 minutes in 2x loading buffer before being subjected to SDS/PAGE.

Scratch wound healing assays:

Cells were plated in 6-well cell culture plates and grown to near confluent monolayers. Scratch wounds were introduced in a cross pattern with a 200 µL

pipette tip. For assays with inhibitors, compounds were added at the indicated concentrations after the scratch wound was introduced. Phase contrast images were taken to the left and/or right of the center of the cross wound after media was replaced and were followed over time. Initial wound area and area after indicated time points were calculated using the Scratch Assay Analyzer tool in the MiToBo plugin for ImageJ 2.0 with $\sigma = 2$ and entropy filter size = 25. The fraction of wound closure was calculated by dividing the final wound area by the initial wound area and subtracting the resulting value from 1. For MCF-10A cell lines, the assay was performed in media supplemented with 20ng/mL EGF. For MCF-10A cell lines with a *PIK3CA* E545K mutation, EGF free media conditions were used. MCF7 and MCF7 corrected derivatives were assayed in 10% serum supplemented media.

Microchannel migration assays:

Standard photolithography and replica molding were used to create the polydimethylsiloxane (PDMS) microfluidic device designed for studying cell migration, as previously described (45-48). Arrays of microchannels that are 200μm long, 10μm tall, and have widths of 50μm, 20μm, 10μm, 6μm, or 3μm were connected at one end to a channel for cell seeding and at the other end to a channel containing a chemoattractant. 6mm diameter inlets and outlets were punched in the PDMS device to allow the addition of media and cells. The PDMS device and a glass coverslip were plasma cleaned, and the PDMS device was adhered to the glass surface. Collagen Type I (BD Biosciences) at 20μg/mL in phosphate buffered saline (PBS) was absorbed for one hour at 37^{o}C. Prior to the

addition of cells, the collagen solution was aspirated and the device was washed with PBS. 50,000 cells in 50μL of serum-free media were added to the cell inlet of the microfluidic device. Cells align at the entrance to microchannels and a chemotactic gradient is established along the microchannels. For MCF-10A derivatives, a gradient of media containing no to 5% horse serum was established, while for MCF7, a gradient of media containing no to 10% FBS was used. Cell migration was observed by time-lapse microscopy at 10 min intervals for 12 hours or more. In each frame, the xy position of a cell was defined by the central cell body. Cellular velocity, displacement, and distance traveled were calculated by a custom MATLAB program. Data are representative of ≥30 tracked cells per cell line and at least three independent experiments.

Flow cytometry and extracellular staining:

$1x10^6$ cells were treated with Human TruStain FcX Fc receptor blocking solution (BioLegend, San Diego, CA) before staining. Data were collected using a FACSCalibur II and analyzed using FACSComp software (BD Biosciences). Gates and quadrants were set based on isotype control staining. The following fluorochrome labeled antibodies were used: APC anti-human CD340 (erbB2/HER-2) (324407; BioLegend), PE anti-human erbB3/HER-3 antibody (324705; BioLegend), APC mouse IgG1, κ isotype control (FC) antibody (400121; BioLegend), and PE mouse IgG2a, κ isotype control (FC) antibody (400213; BioLegend).

Xenograft assays:

For each group, at least five 8- to 10-week-old female athymic nude mice (Harlan Laboratories, Indianapolis, IN) with or without estrogen pellet supplementation as noted were injected subcutaneously in either flank with 200 µl mixture containing $2x10^6$ cells in 20% PBS and 80% growth factor reduced Matrigel (BD Biosciences). Tumor volumes were analyzed weekly and calculated by multiplying length, width, and height for each individual tumor.

For tail vein injection assays, $1x10^5$ cells in 200 µl of PBS were injected into the tail vein of 8- to 10-week-old female athymic nude mice. After 5 weeks, animals were euthanized and their lungs were excised and fixed in 10% formalin and embedded in paraffin, cut into sections and stained with hematoxylin and eosin. Lungs were examined grossly, and five stained sections were examined for evidence of multicellular, proliferating disease per experimental group under a phase contrast microscope.

All animal experiments were performed in accordance with institutional and The National Institutes of Health Guide for the Care and Use of Laboratory Animals guidelines

Statististics:

All statistical analyses were performed using GraphPad Prism 5 software (GraphPad Software). Unpaired Student's T tests, 1-way ANOVA, and 2-way ANOVA tests were used to compare experimental groups to the appropriate

control. Significance levels are indicated using one or more asterisks: $P \leq 0.05$ (*), $P \leq 0.01$ (**), and $P \leq 0.001$ (***). Error bars represent ± SEM.

3 Results

Targeted knock in of single copy, heterozygous *HER2* missense mutations in HER2 non-amplified human breast epithelial cell lines

In order to model *HER2* missense mutations as found in human cancers, we used adeno-associated virus (AAV)-mediated gene targeting to create an isogenic panel of *HER2* mutant knock in MCF-10A and MCF7 human breast epithelial cells. These two cell lines do not overexpress or have amplification of *HER2*, thus heterozygous knock in cell lines contain one wild type and one mutant copy of *HER2*, and express HER2 protein at levels consistent with HER2 non-amplified tumors (Figure 1A) (49). Three AAV gene-targeting vectors were used as backbone vectors to introduce each of seven previously reported mutations into the extracellular or kinase domains of *HER2* (Figure 1 and Table 4). Two heterozygous *HER2* mutant clones were generated for each *HER2*

mutation. We also generated wild type control clones using wild type AAV vector backbones for both MCF-10A and MCF7. Cell lines were verified to have a single integrated copy of the desired mutation and equivalent expression of the mutant and wild type alleles using PCR and RT-PCR followed by Sanger sequencing (Figure 2).

HER2 V777L mutation increases HER2 signaling pathway activation in non-transformed MCF-10A cells

Overexpression studies have identified that *HER2* mutations, including G309A, S310F, L755S, V777L, and R896C activate HER2 signaling and promote transformation. To assess whether these effects could be recapitulated in genome edited clones, we initially performed western blotting analysis on our MCF-10A isogenic panel. MCF-10A is a non-transformed human breast epithelial cell line with a mostly diploid karyotype that requires EGF supplementation for proliferation in culture (50). Using genome editing, we have demonstrated that MCF-10A cells can be transformed by the introduction of oncogenic mutations both *in vitro* and *in vivo* (38).

We found that MCF-10A *HER2* V777L cells showed increases in phosphorylation of HER2, EGFR, and ERK compared to control cell lines in 0.2ng/mL EGF (physiologic) (Figure 3) and EGF-free (Figure 4) conditions. No difference in AKT phosphorylation was noted in gene targeted clones (Figure 3 and Figure 4) indicating that activation of the HER2 receptor by this mutation preferentially activates ERK signaling. Interestingly, other *HER2* mutations did not consistently activate HER2 signaling in MCF-10A cells. These results

demonstrate that *HER2* mutations, even those occurring in the same domain of the protein, have distinct effects on signaling pathway activation.

HER2 mutant MCF-10A cells do not exhibit oncogenic properties *in vitro*

Prior overexpression studies identified that *HER2* mutations can lead to transformative changes, including increases in anchorage independent growth and aberrant morphology in three-dimensional culture, even without detectable increases in HER2 phosphorylation (10,30). Therefore, we performed a series of assays to identify transformed properties of our *HER2* mutant cell line panel.

While parental MCF-10A cells require EGF supplementation, EGF independence has been demonstrated to be a feature of transformation in MCF-10A cells (39). However, *HER2* mutations did not confer EGF independence (Figure 5A), and there was little difference in proliferation rates between control and *HER2* mutant cells in assay media containing either 0.2ng/mL (physiologic) or 20ng/mL (maintenance dose) EGF (Figure 5B-C).

We next tested the ability of *HER2* mutations to promote anchorage independent growth in MCF-10A cells. Knock in of *HER2* V777L was not sufficient for colony formation in soft agar, although MCF-10A cells that overexpress *HER2* V777L mutant cDNA formed robust colonies in soft agar as previously reported (10) (Figure 6A). Anchorage independent growth in semisolid medium was not observed in other MCF-10A *HER2* mutant cell lines (Figure 6A). Next, we examined acinar morphology of MCF-10A *HER2* mutant knock in cells in three-dimensional culture. All *HER2* mutant knock in cell lines formed spherical

structures with normal polarization similar to controls (Figure 6B). This was distinct from phenotypes observed with overexpression of *HER2* mutant cDNAs, which led to larger, irregular, spiculated structures with abnormal protrusions (Figure 6B).

HER2 V777L and L755S mutations increase HER2 pathway signaling activation in MCF7 cells

While biochemical signaling differences were modest in MCF-10A *HER2* knock in cell lines, we hypothesized that *HER2* missense mutations may be highly context dependent and require cooperating genetic alterations found in cancer cells to promote additional transformative features. Therefore, we created an isogenic panel of *HER2* mutant MCF7 cell lines containing single copies of *HER2* mutations. The parental MCF7 cell line is derived from a metastatic pleural effusion in a patient with ER-positive breast cancer and does not overexpress HER2 protein. Two *HER2* kinase domain mutations, L755S and V777L, and one extracellular domain mutation, G309A, were chosen for genome editing in MCF7 cells since these mutations have been characterized via overexpression studies to result in increased pathway activation, oncogenic phenotypes, and, in the case of L755S, resistance to lapatinib (10,34). It should be noted that MCF7 contains two copies of an activating E545K *PIK3CA* mutation and one wild type copy of *PIK3CA* (40), a known oncogene involved in PI3 Kinase and MAP Kinase pathway signaling (39).

We initially tested the effects of *HER2* mutations in MCF7 cells by examining signaling pathway activation. Consistent with the results in the MCF-

10A background, MCF7 *HER2* V777L cells showed increases in phosphorylation of HER2, EGFR, and ERK compared to parental MCF7 and control cells in serum starved conditions (Figure 7A) and HER2 in serum supplemented media (Figure 7B). Furthermore, the L755S mutation increased activation of HER2 signaling pathway proteins in MCF7 (Figure 7). In addition, MCF7 cells have greater basal expression of HER3 than MCF-10A cells, and MCF7 *HER2* V777L and L755S cell lines exhibited an increase in HER3 phosphorylation (Figure 7). Notably, AKT activation did not differ significantly among MCF7 parental, control, and *HER2* mutant cell lines. Despite this pathway activation, *HER2* mutations did not affect proliferation in MCF7 cells (Figure 7).

HER2 missense mutations cooperate with mutant *PIK3CA* for augmented pathway activation in MCF7 cells

Since MCF7 *HER2* L755S and V777L cells showed greater signaling activation than their MCF-10A counterparts, we hypothesized that mutant *PIK3CA* E545K in MCF7 may cooperate with *HER2* mutations to increase pathway activation and other transformed phenotypes. Numerous studies have implicated *PIK3CA* mutations in transformation and activation of the PI3 Kinase/AKT pathway (39,51). To test this hypothesis, we used genome editing to introduce the *HER2* V777L mutation into MCF7 cells that had previously undergone gene targeting to restore the *PIK3CA* alleles to wild type (referred to as MCF7 corrected) (40). The resulting cells have three wild type copies of *PIK3CA* and a heterozygous *HER2* V777L mutation (referred to as MCF7 corrected + V777L) (Figure 2C).

MCF7 corrected + V777L cells displayed slightly lower levels of phosphorylated HER2, HER3, and ERK compared to MCF7 *HER2* V777L cells, but relatively more than both MCF7 and MCF7 corrected cells (Figure 8). These results suggest that the *HER2* V777L mutation activates the MAP Kinase pathway in MCF7 cells and that mutant *PIK3CA* may augment this signaling, similar to our past studies (39). Interestingly, both MCF7 corrected and MCF7 corrected + V777L cells had dramatically reduced AKT phosphorylation. While it has been shown that the absence of *PIK3CA* mutations in MCF7 cells lowers activation of the PI3 Kinase/AKT pathway (40), it was unexpected that isolated activation of HER2 signaling via the V777L mutation did not lead to any discernable increase in AKT phosphorylation. This result, along with the concurrent increases in ERK phosphorylation, again suggests that V777L *HER2* preferentially activates the MAP Kinase signaling pathway rather than the PI3 Kinase/AKT signaling pathway. MCF7 corrected and its derivatives also grew similarly to each other, but more slowly than MCF7 parental cells in serum starved conditions (Figures 7-9).

Acinar morphology and anchorage independent growth in MCF7 *HER2* mutant cell lines

To determine any morphologic effects of *HER2* mutations in MCF7 cells, we conducted Matrigel assays. All cell lines appeared similar to parental and control cells. When cells were seeded in Matrigel along with the EGFR/HER2 inhibitor lapatinib, there was little to no effect on the size or morphology of the acini (Figure 10).

We then performed soft agar colony formation assays to test the ability of *HER2* mutations to promote anchorage independent growth in MCF7 cells. While MCF7 V777L clones showed a trend toward increased colony number, this was modest relative to controls. Similarly, MCF7 *HER2* G309A and L755S did not differ significantly from controls (Figure 11). Treatment with lapatinib had a strong inhibitory effect on colony size and formation in all tested cell lines, though there were no significant differences between *HER2* knock in clones and controls (Figure 11A). MCF7 corrected + V777L mutant cells did not exhibit transformed phenotypes in *in vitro* assays compared to controls (Figure 11B and Figure 12). These data suggest that while *PIK3CA* mutations may cooperate with *HER2* mutations to accentuate signaling activation in MCF7 cells, this cooperativity is not sufficient to increase anchorage independent growth or promote abnormal acinar morphology.

Cooperativity between *HER2* and *PIK3CA* mutations leads to increased signaling activation in MCF-10A cells

Since the effects of *HER2* missense mutations as single copies were greater in MCF7 cells compared to MCF7 corrected cells, we wanted to confirm that activating E545K *PIK3CA* mutations in MCF7 *HER2* mutant cells contributed to the observed effects. Therefore, we created *PIK3CA* and *HER2* double mutant cell lines by knock in of the *PIK3CA* E545K mutation into our MCF-10A *HER2* L755S and V777L cell lines. These resultant double knock in cell lines (referred to as L755S DKI and V777L DKI) are heterozygous for their respective *HER2* mutation and for the *PIK3CA* E545K mutation.

We first analyzed activated signaling pathways via western blot in DKI and control cell lines in media with 0.2ng/mL or without EGF. It has been previously demonstrated that MCF-10A cells with knock in of *PIK3CA* E545K (referred to as MCF-10A + E545K) activated both the PI3 Kinase and MAP Kinase pathways compared to MCF-10A parental cells (38,39). MCF-10A HER2 V777L cells had increased levels of HER2 phosphorylation compared to MCF-10A + E545K cells but had similar levels of ERK phosphorylation (Figure 13 and Figure 14). Additionally, both L755S DKI and V777L DKI cell lines showed increases in HER2, EGFR, and ERK phosphorylation compared to MCF-10A + E545K cells and in ERK activation compared to their respective single *HER2* mutation knock in cell lines in media supplemented with 0.2ng/mL EGF (Figure 13A). Differences in EGFR phosphorylation were less apparent in EGF free media conditions (Figure 14A). The DKI cell lines also showed slight increases in AKT phosphorylation compared to *PIK3CA* single knock in cells in EGF free conditions (Figure 14A), but not in the presence of 0.2ng/mL EGF (Figure 13A). Interestingly, there was an increase in the ratio of phosphorylated HER2 to total HER2 in L755S DKI and V777L DKI cells compared to their respective single knock in cell lines in EGF free conditions, which was also present in both L755S DKI and one of two V777L DKI cell lines in 0.2ng/mL EGF conditions (Figure 13B and Figure 14B). Although HER2 is classically considered upstream of PI3K, these results indicate that under certain conditions interactions between mutant *PIK3CA* and mutant *HER2* may lead to “rewiring” and dysregulation of signaling

pathways. Similar pathway dysregulation has been reported in other studies (39,52,53).

Because *PIK3CA* mutations have been shown to confer EGF-independent growth properties to MCF-10A cells, we tested if *HER2* mutations could augment this phenotype. L755S and V777L DKI cells proliferate in EGF-free media, but this growth was not increased compared to MCF-10A + E545K cells (Figure 15). Furthermore, the combination of *HER2* and *PIK3CA* mutations did not confer anchorage independent growth to MCF-10A cells, and proliferating colonies were not observed in soft agar assays (Figure 16A). We next seeded the L755S and V777L DKI cell lines in Matrigel to examine their morphology. Both L755S DKI and V777L DKI cells grew with a morphology similar to controls that was not affected by treatment with lapatinib (Figure 16B). Taken together, our results suggest that while signaling pathway activation was increased in DKI cell lines, this is not sufficient to promote transformation in these assays.

HER2 V777L and *PIK3CA* E545K double mutant cell lines have increased migratory capacity *in vitro*

Since *HER2* overexpression and activation of HER2 signaling have been described to lead to increases in cell migration, we next tested the migratory capacity of *HER2* mutant cell lines in scratch wound healing and chemotactic microchannel migration assays. In scratch wound experiments, MCF-10A V777L DKI cells exhibited significantly increased wound closure compared to both MCF-10A + E545K and L755S DKI cell lines. Treatment with lapatinib significantly reduced the migration of V777L DKI cells (Figure 17). L755S DKI cells exhibited

slower wound closure than the MCF-10A + E545K cells, indicating that the ability to promote migration may be unique to the V777L mutation. Single V777L knock in cells did not migrate more quickly than MCF-10A parental or control cells (Figure 19). In accord with these results, the MCF7 *HER2* V777L cell line also showed an increase in wound closure compared to parental control, which was decreased with lapatinib treatment and not present in MCF7 corrected + V777L cells (Figure 18 and Figure 19).

We next examined the migratory capacity of cells with and without *HER2* V777L mutation in collagen-I coated microchannels using a microfluidic device constructed of polydimethylsiloxane (PDMS) (45-48). This device allows for the characterization of single cell migration, rather than the collective migration observed during wound closure. Individual cells migrate up a chemotactic gradient inside 10μm tall channels of prescribed widths. Because all tested cells do not efficiently migrate through narrow channels (10μm wide or less) we focused our quantitative analysis on cells migrating in 50μm and 20μm wide channels (46).

MCF-10A V777L DKI cells displayed higher migration velocity and persistence (defined as the ratio of net cell displacement to total distance traveled) inside the 50μm channels compared to MCF-10A + E545K cells (Figure 20A). Similarly, MCF7 V777L cells exhibited an increased migratory propensity compared to parental MCF7 (Figure 20B). Although both MCF-10A V777L DKI and MCF7 V777L migrated faster than their corresponding controls in 20μm wide channels, no significant difference was detected in persistence (Figure 20). MCF-

10A cells with a *HER2* V777L mutation, but not a *PIK3CA* E545K mutation did not migrate more quickly than either parental MCF-10A or MCF-10A + E545K cells (Figure 21). Taken together, these studies demonstrate that *HER2* V777L cooperates with the *PIK3CA* E545K to confer increased migratory potential in breast epithelial cells.

HER2 missense mutations do not lead to increased tumor growth or invasion *in vivo*

The ability of *HER2* mutations to increase tumor formation and xenograft growth was tested (Figure 22A). MCF7 *HER2* mutant cell lines did not differ significantly in their growth compared to controls. Additionally, *HER2* mutations did not confer the ability for MCF7 cells to grow without estrogen supplementation in nude mice (Figure 22B). While MCF-10A + E545K cells do not form tumors, prior studies have shown that MCF-10A cells with double knock in of *PIK3CA* and *KRAS* mutations can cooperate to promote tumor formation. Since we observed cooperativity between *PIK3CA* and *HER2* mutations in MCF-10A cells, we also tested the ability of L755S and V777L DKI cell lines to form tumors. However, these cell lines did not form tumors *in vivo* after twelve weeks (Table 5).

Our *in vitro* experiments revealed an increased migratory potential for *HER2* V777L DKI cells, therefore we performed a tail vein injection assay to test the *in vivo* invasiveness of MCF7 *HER2* mutant cell lines. MCF7 is a cell line with low metastatic capability and infrequently forms disease sites in the lungs after injection into the bloodstream through the tail vein (54,55). *HER2* mutant cell

lines did not form any sites of proliferating, multicellular disease in the lungs of nude mice as determined by gross and microscopic inspection (Figure 23). Overall, these results differ from the predicted effects from overexpression experiments of V777L and G309A mutations in MCF7 cells, which formed tumors that grew significantly faster than wild type *HER2* overexpression (10). These results suggest that knock in models of *HER2* mutations may reveal different roles for these mutations in tumor growth when expressed from their endogenous loci and that additional oncogenic alterations are required to impart invasive phenotypes to *HER2*/*PIK3CA* mutant cells.

HER2 and *PIK3CA* mutations cooperate to increase interaction between HER3 and p85

We examined potential interactions in the HER2 signaling pathway that may be responsible for the cooperative effects of *HER2* and *PIK3CA* mutations. Previous work has shown that overexpression of *HER2* in cells with *PIK3CA* mutations enhance HER2-mediated signaling through HER3 and p85 (56). Using the MCF7 cell line panel, we performed immunoprecipitation assays to examine the effect of *HER2* and *PIK3CA* mutations on HER3/p85 dimerization. MCF7 *HER2* L755S and V777L cells showed an increase in HER3-p85 interaction relative to *HER2* and *PIK3CA* wild type cells (Figure 24). Because HER3 levels are significantly lower in MCF-10A cells, this precluded our ability to perform immunoprecipitation assays in our MCF-10A cell line panel. Therefore, we overexpressed mutant or wild type *HER2* and *PIK3CA*, along with wild type *HER3* in HEK293T cells to examine the consequences of their interactions in

another cellular background. Similar to our results with MCF7 cells, the presence of HER3-p85 dimers increased in cells transfected with both V777L *HER2* and E545K *PIK3CA* compared to wild type controls (Figure 25). This increase in HER3-p85 interaction in V777L mutant cells may represent a potential signaling pathway "rewiring" leading to increased MAP Kinase activation via HER3/PI3 Kinase interaction as we have previously described (57). These results suggest that the V777L *HER2* missense mutation in combination with *PIK3CA* mutations increase the formation of HER3-p85 dimers and may be a potential mechanism of increased MAP Kinase pathway signaling.

HER2 mutations and proliferative response to HER2 targeted therapies

Given that overexpression models of *HER2* mutations revealed differential sensitivities to HER2 targeted drugs, we measured the IC_{50} values of two HER2/EGFR tyrosine kinase inhibitors, lapatinib and neratinib, on our isogenic *HER2* knock in cell line panel (Supplemental Tables 3-4 and Supplemental Figure 8) (10,34).

For MCF-10A cells, ~650-1000 nM lapatinib was necessary to inhibit cell proliferation for cells regardless of *HER2* and/or *PIK3CA* mutation status (Table 6, Figures 26A and 27A). While MCF7 cells were relatively insensitive to lapatinib, *HER2* mutations again did not alter the response to lapatinib (Table 6 and Figures 28A and 29A). Interestingly, cells harboring a *HER2* L755S mutation did not exhibit resistance to lapatinib in terms of proliferation or biochemical pathway activation (Table 7 and Figure 31). Similar to the results of lapatinib treatment, *HER2* mutations did not predict for substantial sensitivity or resistance

to neratinib in our cell line models. However, neratinib was slightly more potent in L755S DKI cell lines compared to control (Table 7 and Figure 27B). This sensitivity was not found in MCF-10A *HER2* L755S or MCF7 *HER2* L755S backgrounds (Table 7 and Figures 26B and 28B). Moreover, all cell lines were relatively insensitive to trastuzumab at doses up to 100μg/mL, perhaps due to the poor anti-signaling effect and complex mechanism of action of trastuzumab (data not shown) (20). Additionally, cell lines with both a *PIK3CA* and a *HER2* mutation were not more sensitive to the PI3K p110α specific inhibitor BYL-719 than cells with a single *PIK3CA* mutation. As expected, cells without a *PIK3CA* mutation were relatively resistant to BYL-719 (Table 8 and Figure 30).

Cell Line	Description
MCF-10A	Parental MCF-10A cell line
MCF-10A *HER2* G309A	MCF-10A with single *HER2* G309A knock in allele
MCF-10A *HER2* S310F	MCF-10A with single *HER2* S310F knock in allele
MCF-10A *HER2* L755S	MCF-10A with single *HER2* L755S knock in allele
MCF-10A *HER2* I767M	MCF-10A with single *HER2* I767M knock in allele
MCF-10A *HER2* V777L	MCF-10A with single *HER2* V777L knock in allele
MCF-10A *HER2* Y835F	MCF-10A with single *HER2* Y835F knock in allele
MCF-10A *HER2* R896C	MCF-10A with single *HER2* R896C knock in allele
MCF-10A Targeted WT 1	MCF-10A with wild type vector knock in allele
MCF-10A Targeted WT 2	MCF-10A with wild type vector knock in allele
MCF-10A Targeted WT 3	MCF-10A with wild type vector knock in allele
MCF-10A + E545K	MCF-10A with single *PIK3CA* E545K knock in allele
MCF-10A L755S DKI	MCF-10A *HER2* L755S with single *HER2* E545K knock in allele
MCF-10A V777L DKI	MCF-10A *HER2* V777L with single *HER2* E545K knock in allele
MCF7	Parental MCF7 cell line
MCF7 *HER2* G309A	MCF7 with single *HER2* G309A knock in allele
MCF7 *HER2* L755S	MCF7 with single *HER2* L755S knock in allele
MCF7 *HER2* V777L	MCF7 with single *HER2* V777L knock in allele
MCF7 Targeted WT 1	MCF7 with wild type vector knock in allele
MCF7 Targeted WT 2	MCF7 with wild type vector knock in allele
MCF7 Corrected	MCF7 with two *PIK3CA* E545E knock in alleles
MCF7 Corrected + V777L	MCF7 corrected with single *HER2* V777L knock in allele
MCF-10A HER2 WT O/E	MCF-10A overexpressing wild type *HER2* cDNA
MCF-10A HER2 G309A O/E	MCF-10A overexpressing *HER2* G309A cDNA
MCF-10A HER2 L755S O/E	MCF-10A overexpressing *HER2* L755S cDNA
MCF-10A HER2 V777L O/E	MCF-10A overexpressing *HER2* V777L cDNA

Table 1: Cell lines used in this study

Primers Used in This Study		
Homology Arm Cloning Primers		
Targeting Vector	Homology Arm	Forward/Reverse Primer
Vector 1 (L755, I767)	5'	GATTCTGCCCAACTGTAAGC
		TTGCCCCTCCCATCAGAACT
	3'	GAGCTGGAGGCAGTGTTTGG
		CACAGCCTGTGAAGGCTCAA
Vector 2 (V777, Y835, R896)	5'	GAGCTGGAGGCAGTGTTTGG
		CACAGCCTGTGAAGGCTCAA
	3'	GGCCATGGCTGTGGTTTGTGAT
		CCTCAAGAGTGGCTTTGGAC
Vector 3 (G309, S310)	5'	AAGCTCTTAGAACGGTGCCT
		AGAGACTAGGTCCCAAGAGG
	3'	GCCTTCTACTCTCTACCCCT
		GCTGACAGAGTGAGACTCTA
Pre-Cre Screening Primers		
Targeting Vector	Homology Arm	Forward/Reverse Primer
Vector 1 (L755, I767)	5'	GGTGGAAAGACTGCTTGAGC
		GCAGACAGCGAATTAATTCC
	3'	GCATACATTATACGAAGTTATCCAA
		ACACCAGCCATCACGTATGC
Vector 2 (V777, Y835, R896)	5'	CCTGAAAGAGACGGAGCTGA
		GCAGACAGCGAATTAATTCC
	3'	TTAAGGTACCACTGTGCATATG
		AGACACCAACTCCCGGAATC
Vector 3 (G309, S310)	5'	AAGCTCTTAGAACGGTGCCT
		GCAGACAGCGAATTAATTCC
PIK3CA E545K	5'	ATCTCTTTCCTGGACTACTGG
		GCAGACAGCGAATTAATTCC
	3'	TTAAGGTACCACTGTGCATATG
		TAAAATTCAAAAGACATCAGTG
Post Cre Screening Primers		
Targeting Vector	Forward/Reverse Primer	
Vector 1 (L755, I767)	GGTGGAAAGACTGCTTGAGC	
	AGAAGGCGGGAGACATATGG	
Vector 2 (V777, Y835, R896)	CCTGAAAGAGACGGAGCTGA	
	CATATGCACAGTGGTACCTTAA	
Vector 3 (G309, S310)	AAGCTCTTAGAACGGTGCCT	
	CATATGCACAGTGGTACCTTAA	
PIK3CA E545K	ATCTCTTTCCTGGACTACTGG	
	CATATGCACAGTGGTACCTTAA	

Table 2: Primers used in this study

Bi-Allelic Sequencing Primers		
Targeting Vector	Forward/Reverse Primer	Nested Sequencing
Vector 1 (L755, I767)	GAGCTGGAGGCAGTGTTTGG	
	CACAGCCTGTGAAGGCTCAA	GCAGTGAGCCGAGATAACGC
Vector 2 (V777, Y835, R896)	GGCCATGGCTGTGGTTTGTGAT	
	CCTCAAGAGTGGCTTTGGAC	ATGGGCTAGACACCACTCCA
Vector 3 (G309, S310)	AAGCTCTTAGAACGGTGCCT	
	AGAGACTAGGTCCCAAGAGG	CAGGCATGCACCACCATGGC
PIK3CA E545K	TGAAAATAAAGTCTTGCAATG	
	TTAGGCACAGTTATAATGGC	AGTAACAGACTAGCTAGAGA
Targeted Allele Sequencing Primers		
Targeting Vector	Forward/Reverse Primer	Nested Sequencing
Vector 1 (L755, I767)	GGTGGAAAGACTGCTTGAGC	
	AGAAGGCGGGAGACATATGG	TTAAGGTACCACTGTGCATATG
Vector 2 (V777, Y835, R896)	TTAAGGTACCACTGTGCATATG	
	TGGCCGACATTCAGAGTCAA	GGTCTTTCCCTAATCCTGGG
Vector 3 (G309, S310)	AAGCTCTTAGAACGGTGCCT	
	TGGCCGACATTCAGAGTCAA	TGCTGCTCATGGTGGTGCAC
Mutagenesis Primers		
Mutation	Forward/Reverse Primer	
G309A	CGGACGTGGcATCCTGCACC	
	GGTGCAGGATgCCACGTCCG	
S310F	ACGTGGGATtCTGCACCCTC	
	GAGGGTGCAGaATCCCACGT	
L755S	GGCCATCAAAGTGTcGAGGGAAAACACATC	
	GATGTGTTTTCCCTCgACACTTTGATGGCC	
I767M	GCCAACAAAGAAATgTTAGACgtaagcccc	
	ggggcttacGTCTAAcATTTCTTTGTTGGC	
V777L	TACGTGATGGCTGGTtTGGGCTCCCCATAT	
	ATATGGGGAGCCCAaACCAGCCATCACGTA	
Y835F	GGGATGAGCTtCCTGGAGGA	
	TCCTCCAGGaAGCTCATCCC	
R896C	GTCCATTCTCtGCCGGCGGT	
	ACCGCCGGCaGAGAATGGAC	
cDNA Sequencing Primers		
Targeting Vector	Forward/Reverse Primer	Nested Sequencing
Vector 1 (L755, I767)	GTGAAGGTGCTTGGATCTGG	
	ATCTGCATGGTACTCTGTCT	GTTGGGACTCTTGACCAGCA
Vector 2 (V777, Y835, R896)	GTGAAGGTGCTTGGATCTGG	
	ATCTGCATGGTACTCTGTCT	GTTGGGACTCTTGACCAGCA
Vector 3 (G309, S310)	GCCTGCCTCCACTTCAACCA	
	GTAACTGCCCTCACCTCTCG	CATCTGTGAGCTGCACTGCC
PIK3CA E545K	CGACTTTGCCTTTCCATTTG	
	GGGTAATTACAGTCCAGAAG	CAGGATTTAGCTATTCCCAC

Table 3: Primers used in this study (continued)

Alteration	Domain	Base Change	Reported Cases
G309A	ECD	c.926G>C	1
S310F	ECD	c.929C>T	30
L755S	Kinase	c.2264T>C	30
I767M	Kinase	c.2301C>G	5
V777L	Kinase	c.2329G>T	11
Y835F	Kinase	c.2504A>T	1
R896C	Kinase	c.2686C>T	3

Table 4: Genomic locus and prevalence as reported in the COSMIC database as of January 2015 for each *HER2* mutation introduced in this study.

Cell Line	Tumors formed	Mice per group
MCF-10A + E545K	0	5
10A + L755S DKI	0	10
10A + V777L DKI	0	10

Table 5: MCF-10A + E545K, L755S, and V777L DKI cells do not form tumors as xenografts in nude mice.

Lapatinib		
Cell Line	**IC_{50} (nM)**	**95% CI**
MCF-10A	665	600-736
MCF-10A Targeted WT	768	684-861
MCF-10A *HER2* G309A	795	725-872
MCF-10A *HER2* S310F	634	565-710
MCF-10A *HER2* L755S	654	596-717
MCF-10A *HER2* I767M	822	745-908
MCF-10A *HER2* V777L	1080	947-1231
MCF-10A *HER2* Y835F	887	808-974
MCF-10A *HER2* R896C	815	718-924
MCF-10A + E545K	1401	1209-1625
MCF-10A L755S DKI	977	893-1068
MCF-10A V777L DKI	1078	799-1206
MCF7	4282	4087-4487
MCF7 Targeted WT	4167	4014-4325
MCF7 *HER2* G309A	4663	4531-4799
MCF7 *HER2* L755S	4154	3996-4319
MCF7 *HER2* V777L	4130	3976-4291
MCF7 Corrected	3784	3539-4046
MCF7 Corrected + V777L	3609	3421-3808

Table 6: Cells were plated on day 0 and lapatinib or DMSO vehicle control was added on day 1. Cell viability and proliferation relative to vehicle control was measured with Alamar Blue on day 6.

Neratinib		
Cell Line	**IC_{50} (nM)**	**95% CI**
MCF-10A	99.8	92.3-107.8
MCF-10A Targeted WT	101.4	92.1-111.8
MCF-10A *HER2* G309A	102.6	94.2-111.6
MCF-10A *HER2* S310F	96.63	88-106.1
MCF-10A *HER2* L755S	76.1	69.4-83.4
MCF-10A *HER2* I767M	111.6	101.7-122.4
MCF-10A *HER2* V777L	124.3	110.4-139.9
MCF-10A *HER2* Y835F	100.1	91.6-109.3
MCF-10A *HER2* R896C	93.5	84.9-102.9
MCF-10A + E545K	153	138.6-168.8
MCF-10A L755S DKI	16.3	15.7-18.3
MCF-10A V777L DKI	93.3	57.3-151.8
MCF7	777.4	697.2-866.8
MCF7 Targeted WT	788.7	732.4-849.3
MCF7 *HER2* G309A	963.5	893.2-103.9
MCF7 *HER2* L755S	787.3	731.1-847.8
MCF7 *HER2* V777L	820.1	759.4-885.8
MCF7 Corrected	889.2	774.8-1020
MCF7 Corrected + V777L	510.8	464-562.3

Table 7: Cells were plated on day 0 and neratinib or DMSO vehicle control was added on day 1. Cell viability and proliferation relative to vehicle control was measured with Alamar Blue on day 6.

BYL-719		
Cell Line	**IC_{50} (nM)**	**95% CI**
MCF-10A	1568	1158-2123
MCF-10A Targeted WT	1093	778-1536
MCF-10A *HER2* L755S	1647	1219-2226
MCF-10A *HER2* V777L	3341	2355-4740
MCF-10A + E545K	180.8	141.5-230.8
MCF-10A L755S DKI	186.4	148.1-234.7
MCF-10A V777L DKI	299.6	230.4-389.6
MCF7	4191	3511-5002
MCF7 Targeted WT	2781	2301-3362
MCF7 *HER2* G309A	2411	2084-2789
MCF7 *HER2* L755S	2915	2543-3342
MCF7 *HER2* V777L	3134	2792-3517
MCF7 Corrected	>10,000	
MCF7 Corrected + V777L	>10,000	

Table 8: Cells were plated on day 0 and BYL-719 or DMSO vehicle control was added on day 1. Cell viability and proliferation relative to vehicle control was measured with Alamar Blue on day 6.

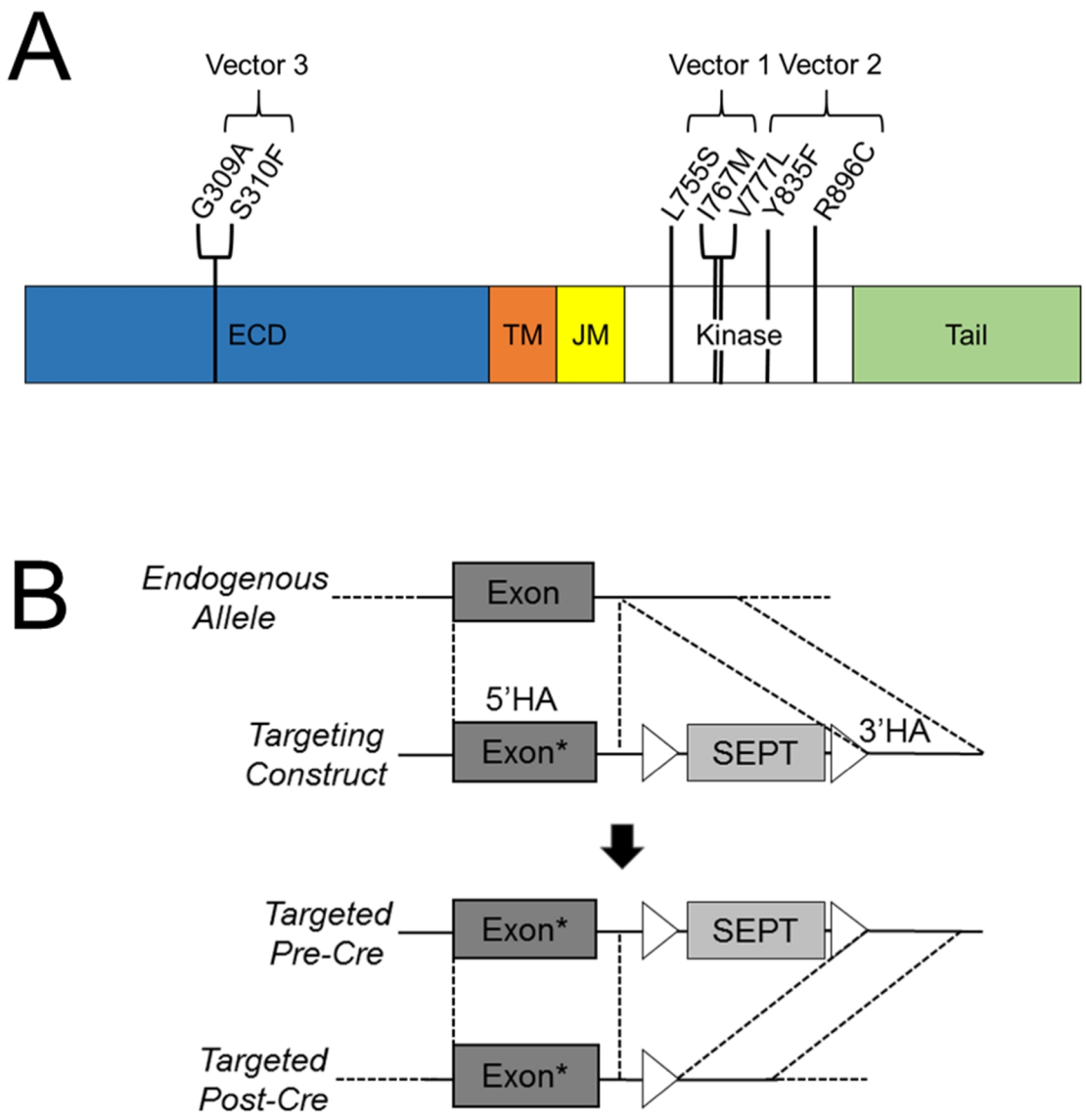

Figure 1: A) Previously identified *HER2* mutations included in the isogenic panel. Three distinct gene targeting vectors were used to introduce the mutations. Abbreviations: ECD, extracellular domain; TM, transmembrane region; JM, juxtamembrane region. B) Representative rAAV-mediated gene targeting strategy for a targeting vector carrying an exonic mutation (*) within the 5' homology arm (HA). rAAV transduction leads to integration of the targeting vector via homologous recombination of the 5' and 3' homology arms (HAs). After neomycin selection and clone isolation, *loxP* (triangles) flanked SEPT cassette is excised using Cre recombinase.

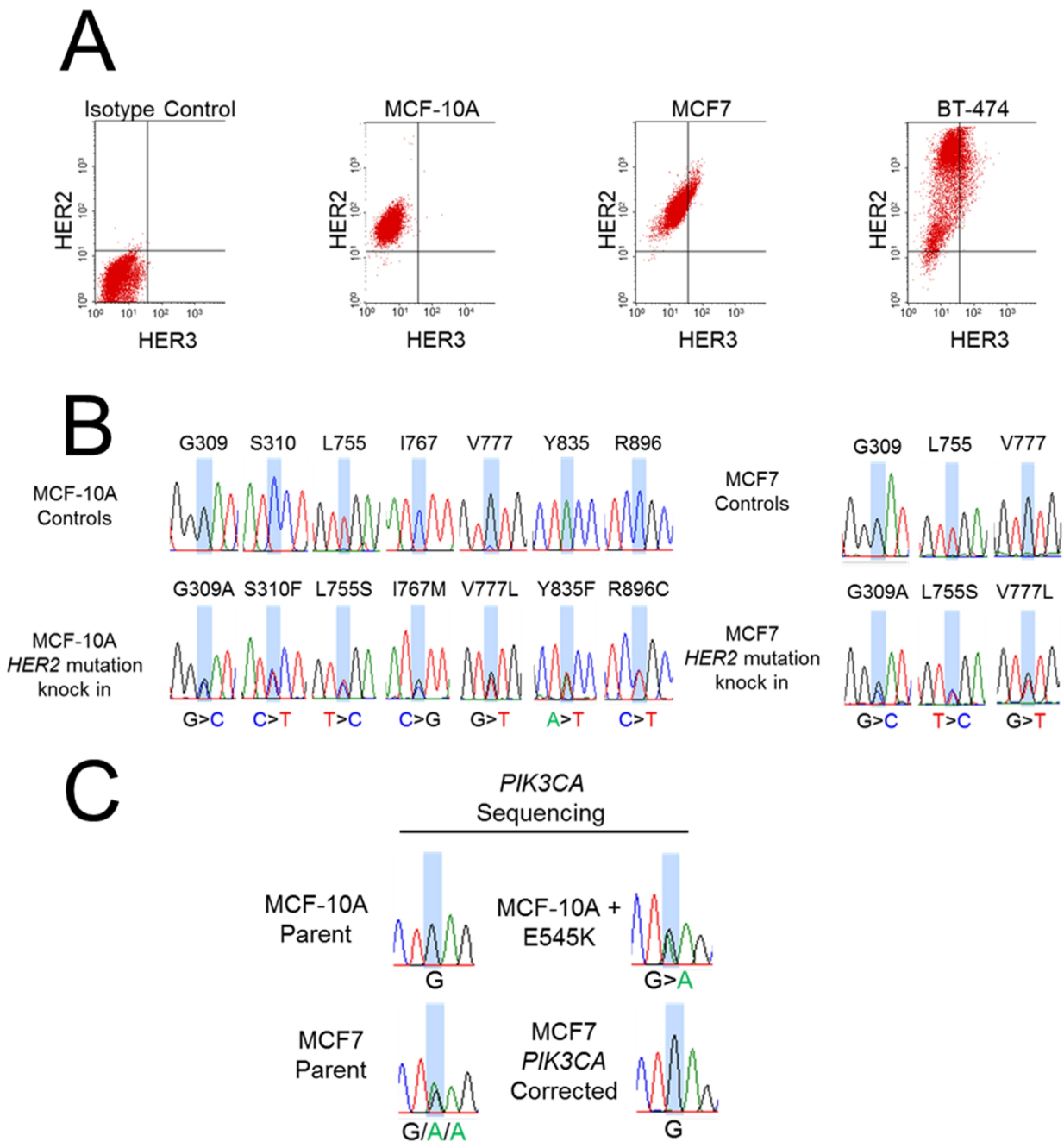

Figure 2: A) MCF-10A and MCF7 parental cell lines were analyzed for expression of HER2 and HER3 cell surface protein by flow cytometry compared to the *HER2*-amplified BT-474 cell line. B) Representative cDNA sequencing traces for MCF-10A and MCF7 parental cell lines (top) and *HER2* heterozygous mutant knock in cell lines (bottom) at the indicated loci. C) Representative cDNA sequencing traces of the *PIK3CA* E545 locus.

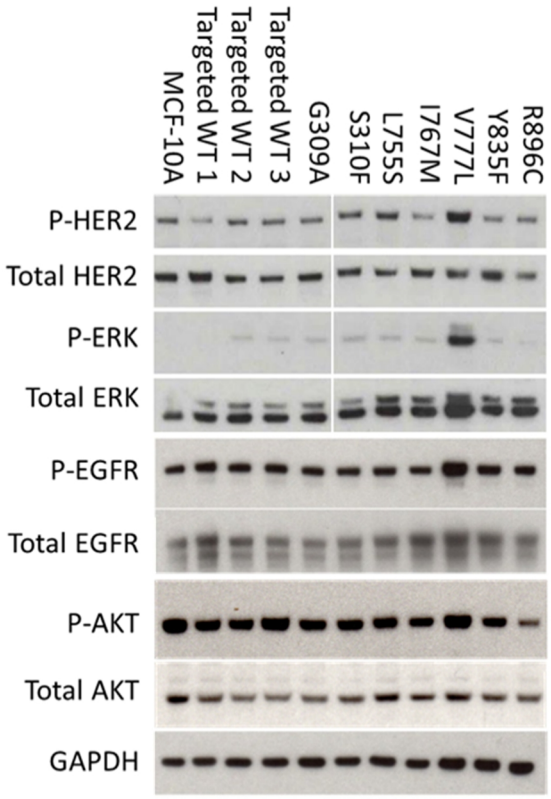

Figure 3: MCF-10A *HER2* mutant and control cell lines were grown in physiologic (0.2ng/mL) EGF supplemented assay media and subjected to western blotting analysis with the indicated antibodies. White lines represent lanes have been removed from blot.

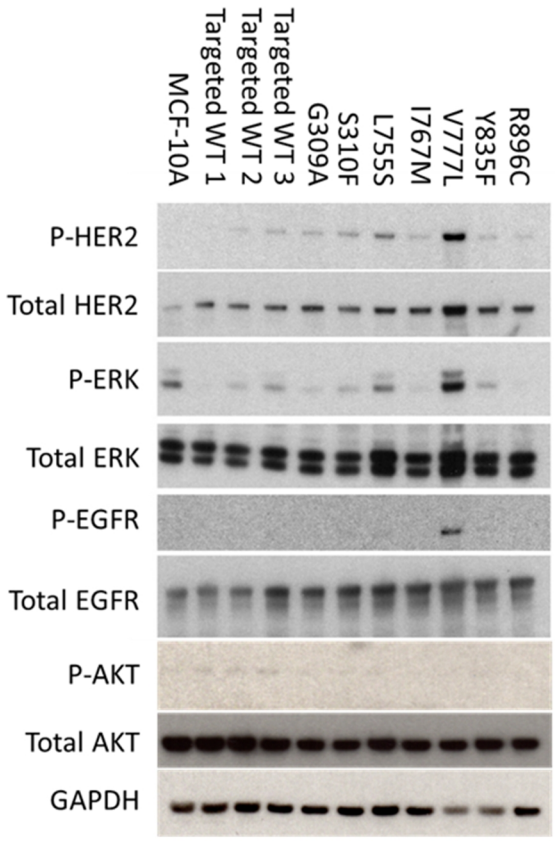

Figure 4: MCF-10A *HER2* mutants and controls were grown in assay media without EGF and subjected to western blotting analysis with the indicated antibodies.

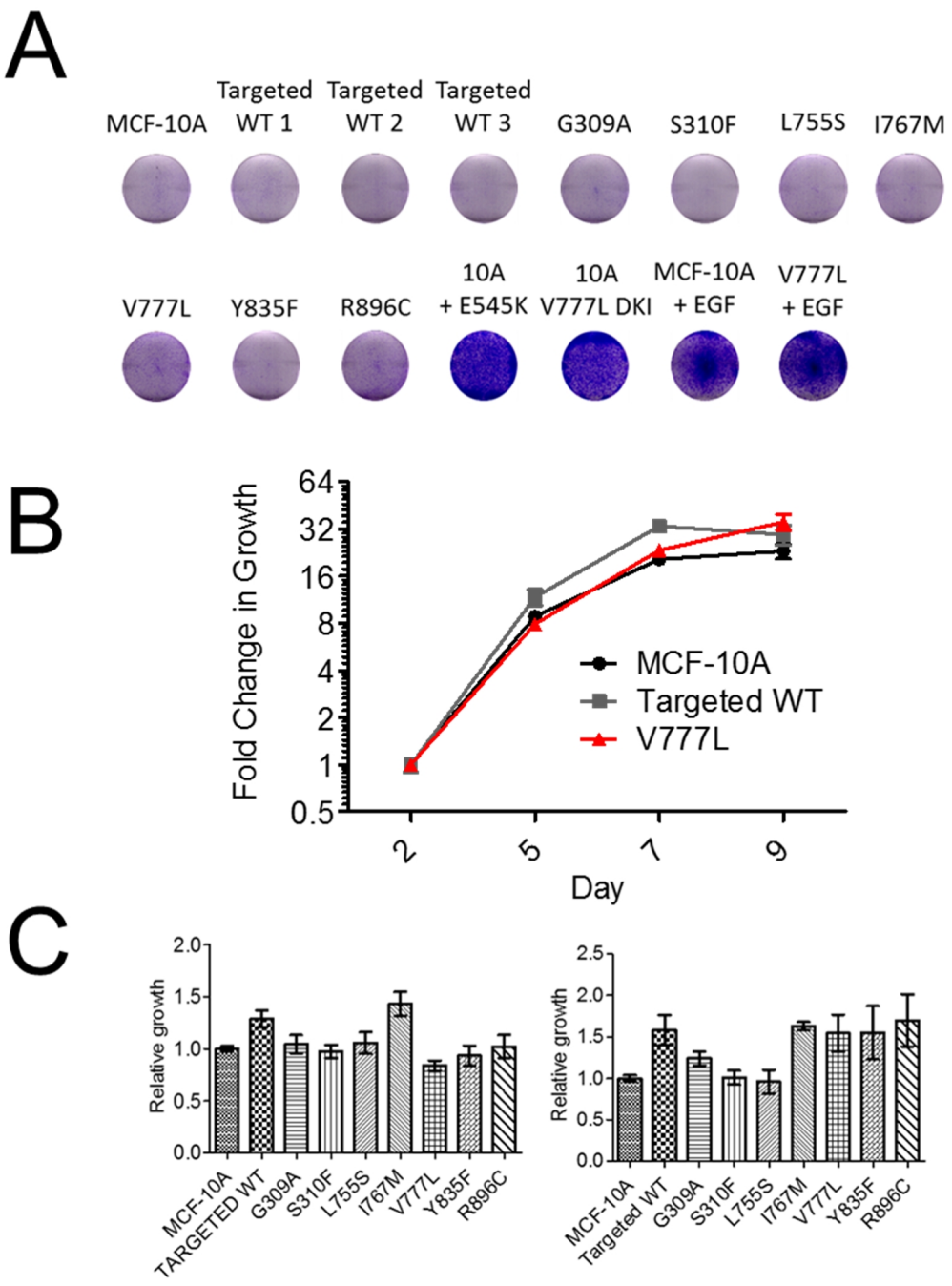

Figure 5: A) 2x10^4 cells were plated in six-well tissue culture plates in assay media without EGF on day 0. Wells were stained with crystal violet on day 6. . B) Relative mean (±SEM) proliferation data for V777L clones and MCF-10A controls in 0.2ng/mL EGF supplemented assay media ($n \geq 6$ per cell line, two independent experiments were performed). C) Mean proliferation relative to MCF-10A parental cells (±SEM) at day 7 for MCF-10A *HER2* mutants and controls in assay media with 20ng/mL (left) or 0.2ng/mL (right) EGF ($n \geq 5$, two independent experiments were performed).

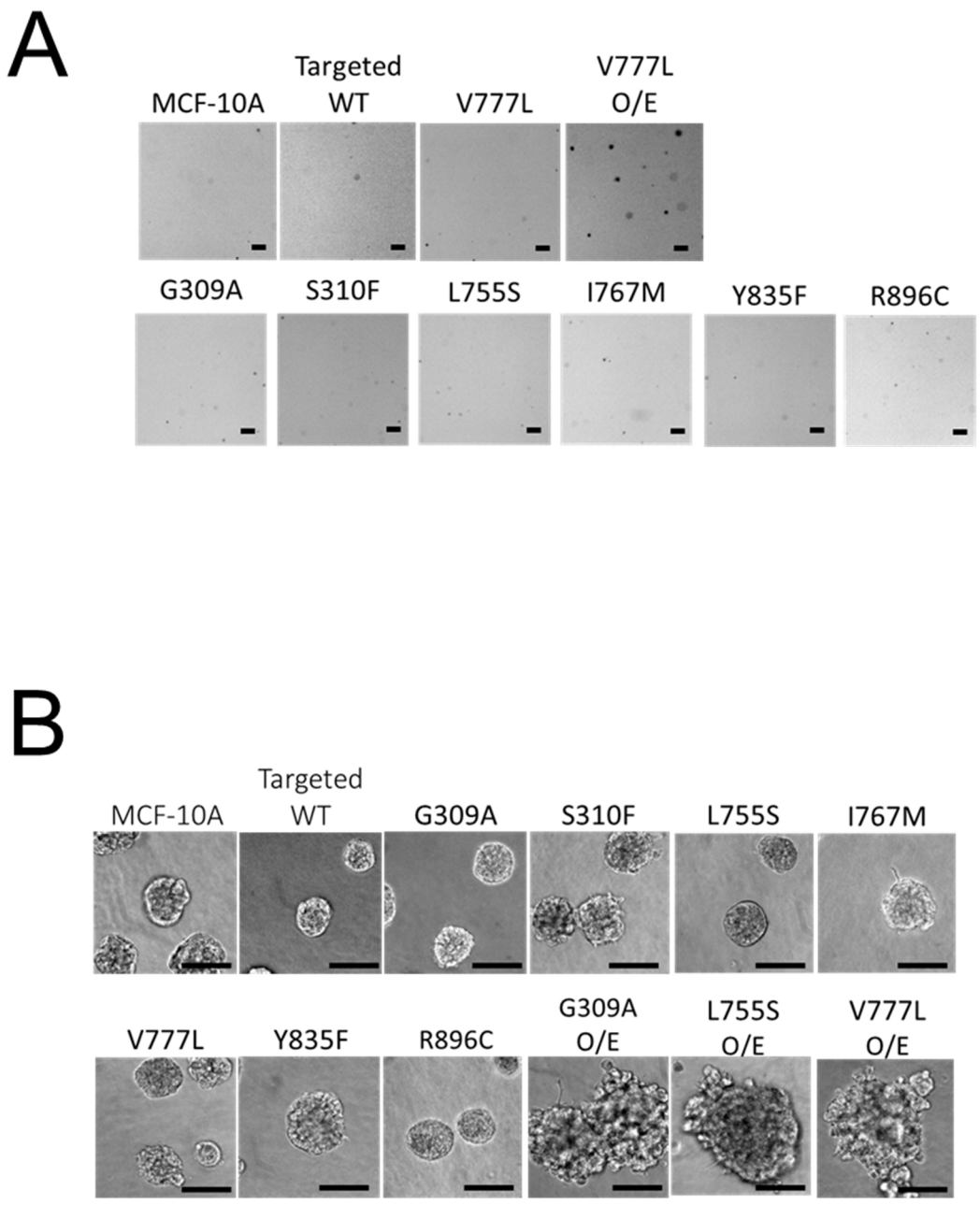

Figure 6: A) Representative images depicting soft agar colony formation for MCF-10A controls, *HER2* mutant isogenic cell lines, and an MCF-10A cell line overexpressing the *HER2* V777L cDNA. Bar = 200μm. B) 3D acinar morphogenesis assay for MCF-10A *HER2* mutant isogenic cell lines and mutant *HER2* overexpression cell lines. Bar = 50μm.

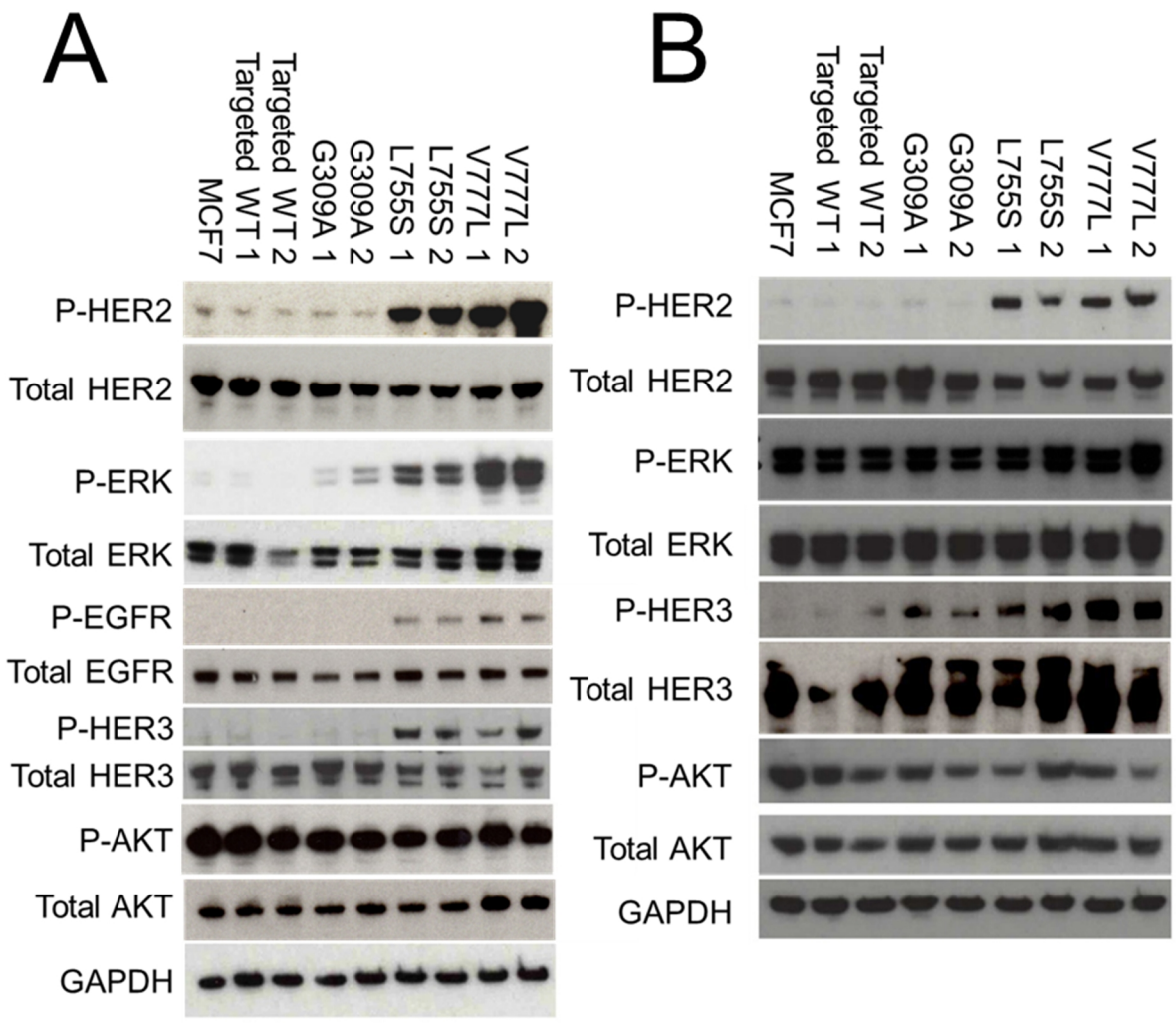

Figure 7: MCF7 *HER2* mutant and control cell lines were grown in serum starved (A) or serum supplemented (B) conditions and subjected to western blotting analysis with the indicated antibodies.

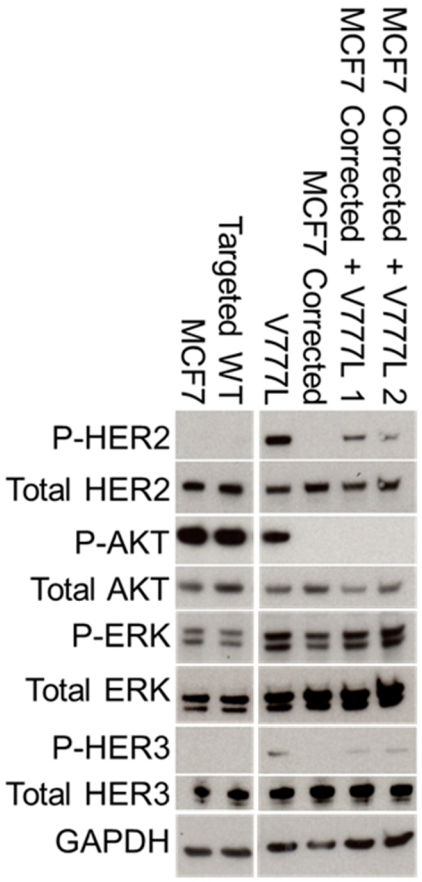

Figure 8: Western blotting analysis of MCF7 and MCF7 corrected cell lines and *HER2* mutant derivatives in serum starved media conditions. White lines represent lanes have been removed from blot.

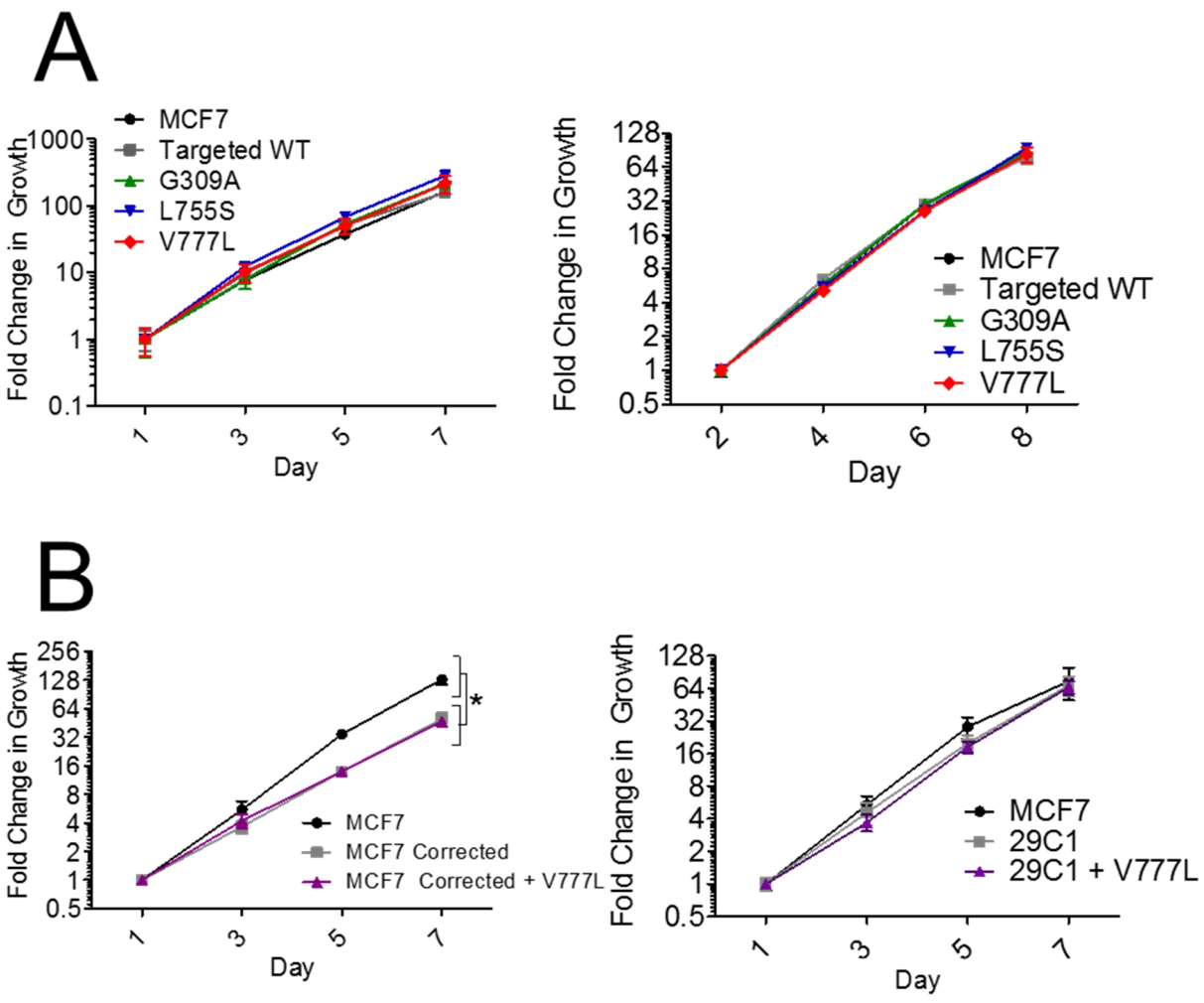

Figure 9: A) Relative mean (±SEM) proliferation for MCF7 *HER2* mutants in serum supplemented (left) or serum starved (right) media ($n \geq 6$, two independent experiments were performed). B) Mean (±SEM) relative proliferation for MCF7, MCF7 corrected, and MCF7 corrected + V777L cells as in serum supplemented (left) or serum starved (right) media conditions ($n \geq 5$, two independent experiments were performed, $^{**}P \leq .01$, 2-way ANOVA followed by Bonferroni multiple comparison test).

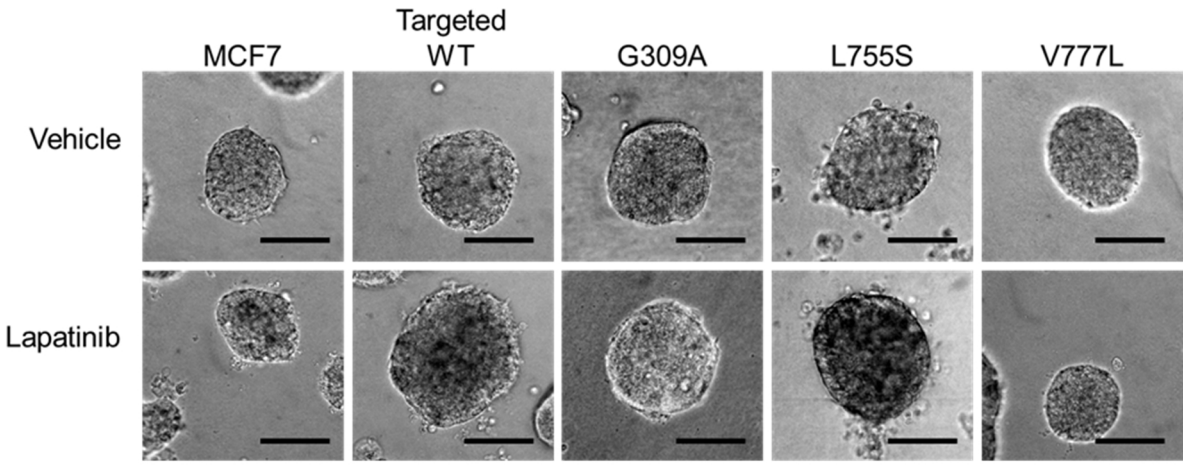

Figure 10: MCF7 control and *HER2* mutant cells were seeded into 3D Matrigel culture in the presence of DMSO vehicle control or lapatinib (5μM) and photographed on day 12. Bar = 100μm.

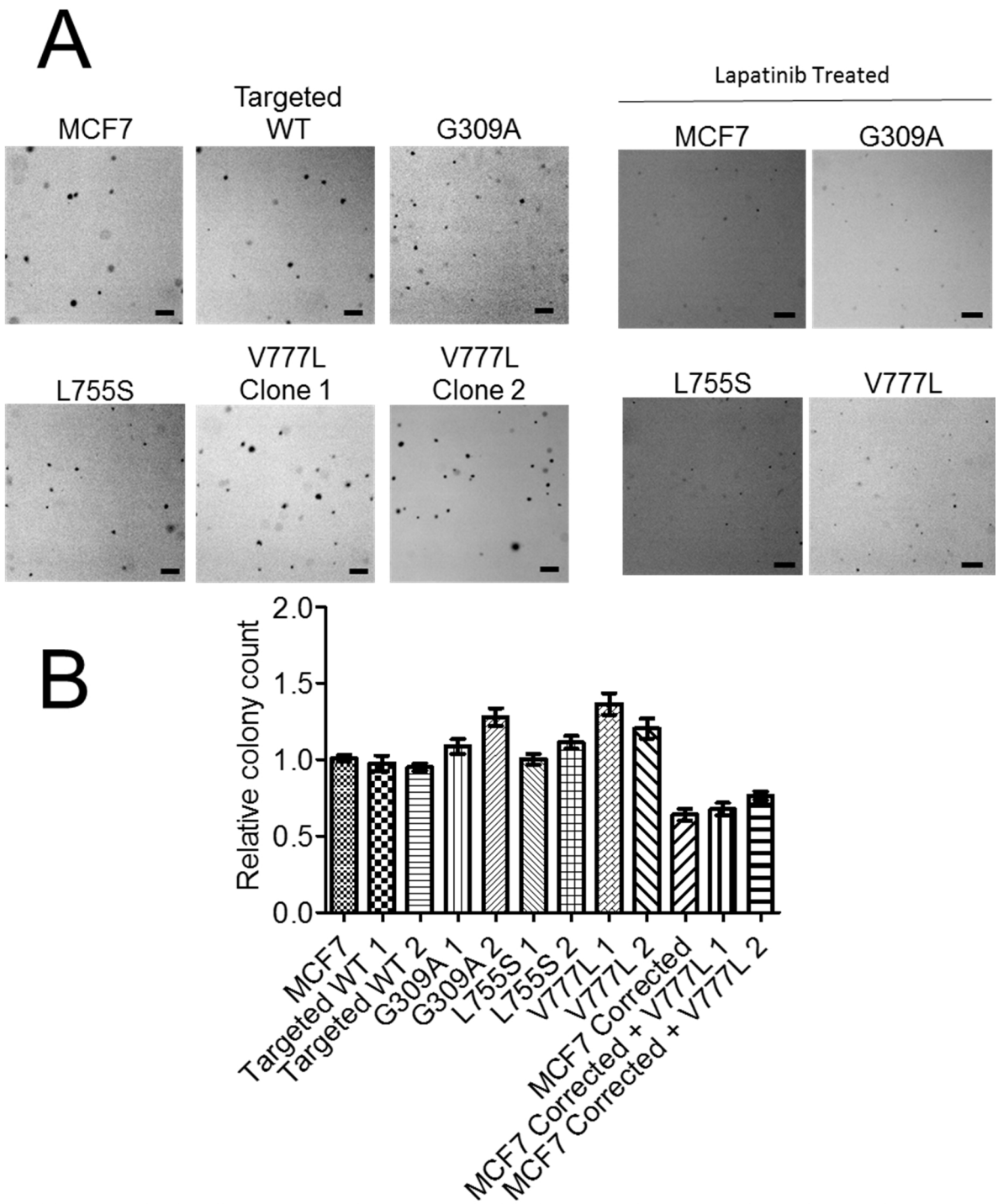

Figure 11: A) Representative images depicting soft agar colony formation in MCF7 *HER2* knock in cell lines and controls (left) and MCF7 *HER2* knock in cell lines treated with 5μM lapatinib (right). Bar = 200 μm. B) Relative mean (±SEM) number of colonies formed in soft agar assays as counted visually via phase contrast microscopy ($n \geq 5$ at least two independent experiments were performed).

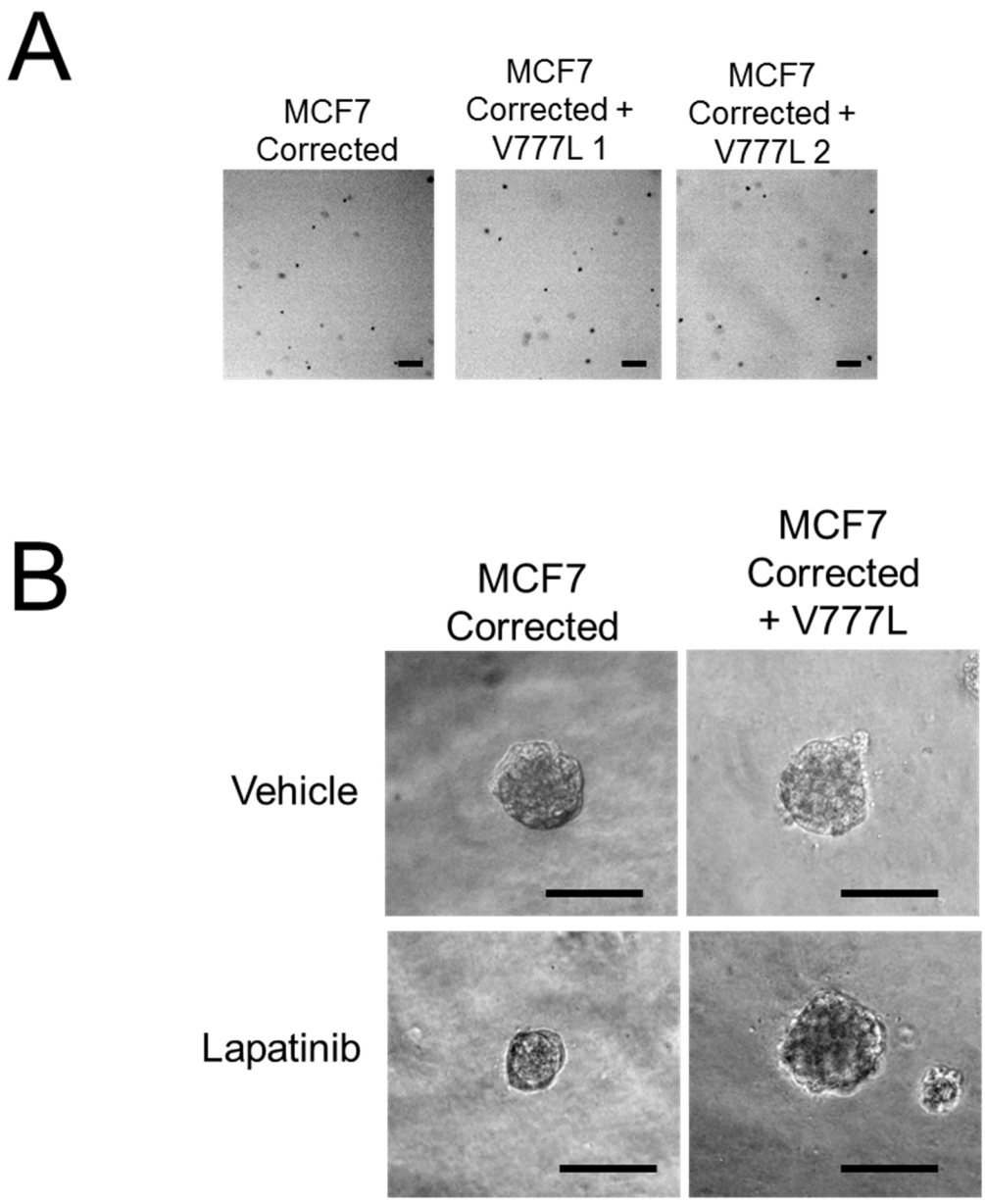

Figure 12: A) Representative images depicting soft agar colony formation in *HER2* mutant MCF7 corrected cell lines and controls after 4 weeks of incubation with DMSO vehicle control. B) MCF7 corrected and MCF7 corrected + V777L cells were seeded into 3D Matrigel culture in the presence of DMSO vehicle or lapatinib (5μM) and photographed on day 12. Bar = 200μm

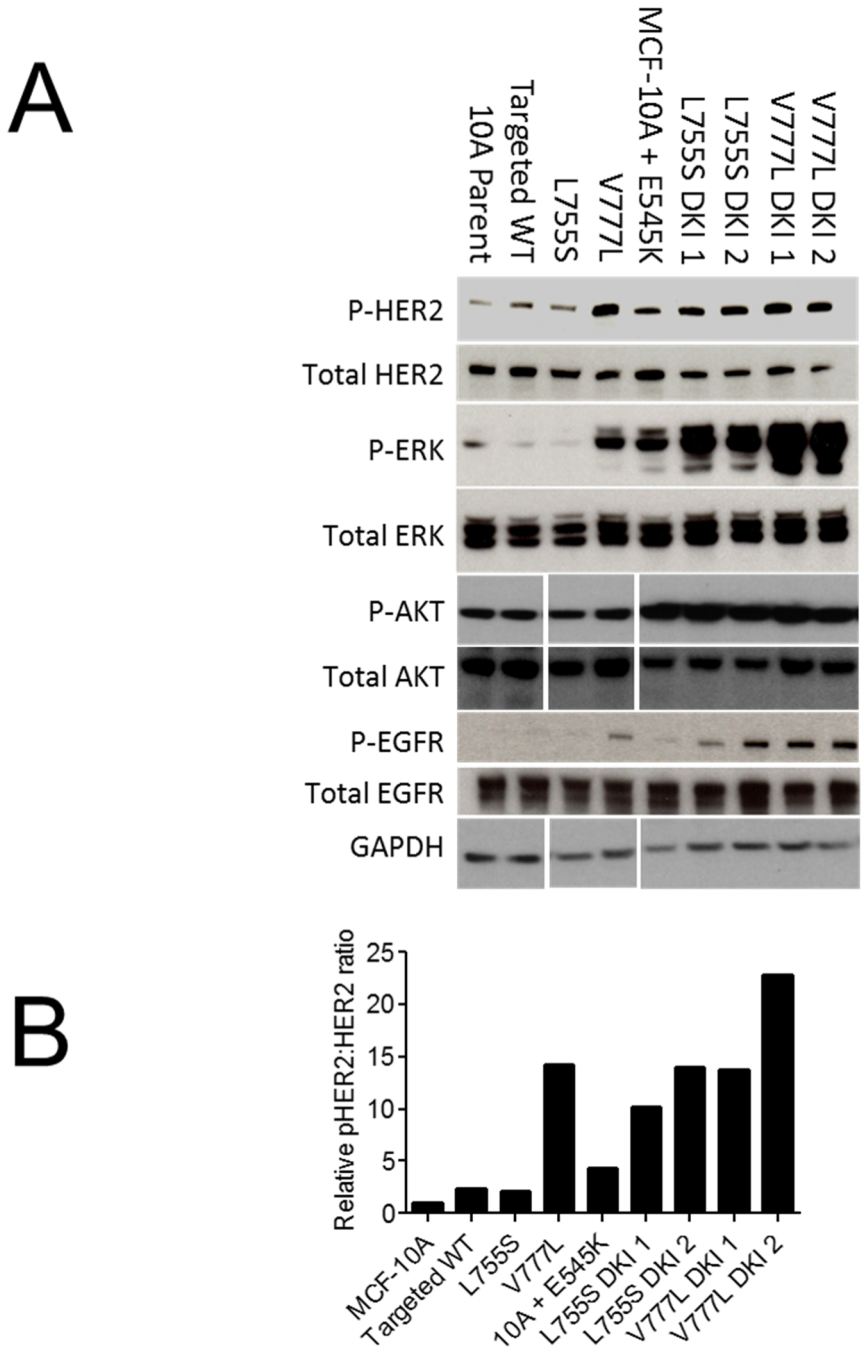

Figure 13: A) MCF-10A *HER2* mutant, L755S DKI, V777L DKI, and control cell lines were grown in physiologic 0.2ng/mL EGF supplemented assay media and subjected to western blotting analysis with the indicated antibodies. White lines represent lanes have been removed from blot. B) Ratio of pHER2 to total HER2 western blot band quantification relative to the MCF-10A parental cell line in 0.2ng/mL conditions as measured with ImageJ software.

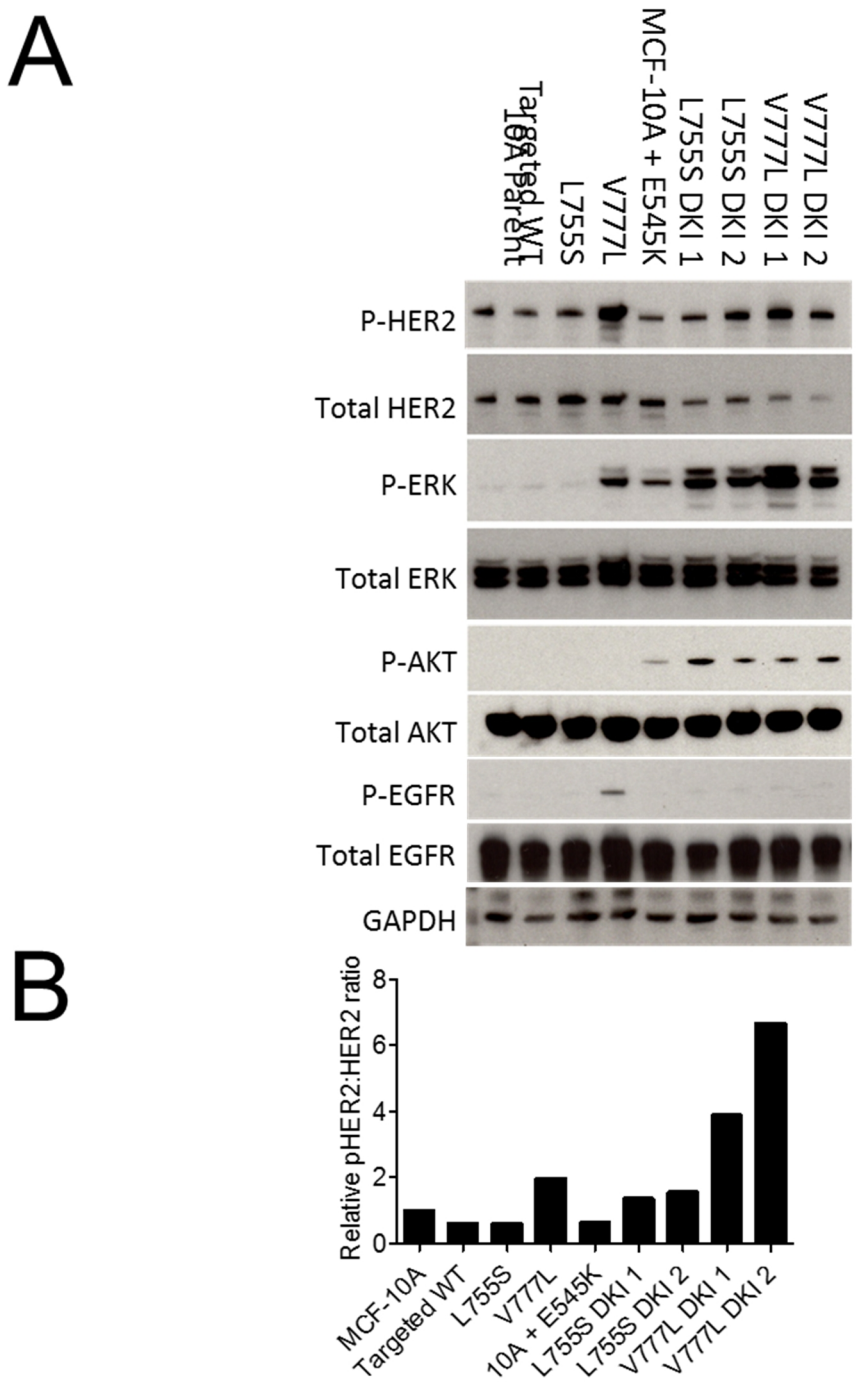

Figure 14: A) MCF-10A *HER2* mutant, L755S DKI, V777L DKI, and control cell lines were grown in EGF free assay media and subjected to western blotting analysis with the indicated antibodies. White lines represent lanes have been removed from blot. B) Ratio of pHER2 to total HER2 western blot band quantification relative to the MCF-10A parental cell line in EGF free conditions as measured with ImageJ software.

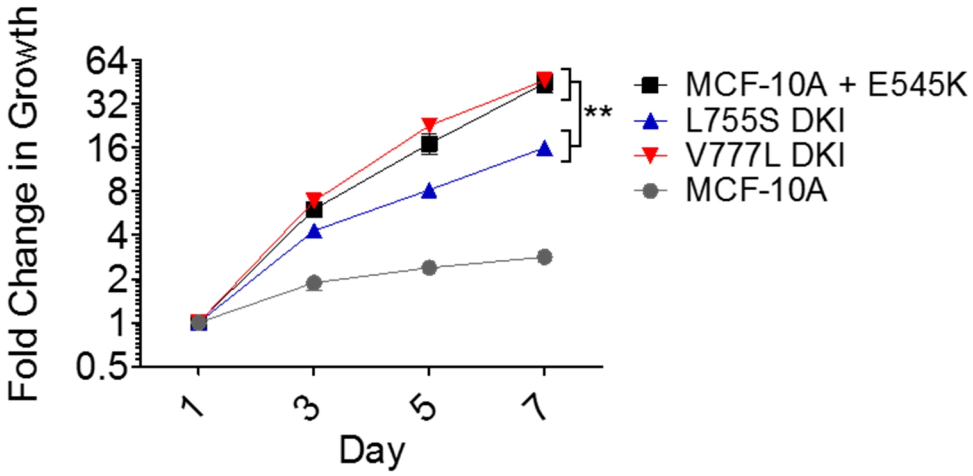

Figure 15: Relative proliferation in assay media without EGF. Data are representative of the mean (±SEM) relative to each cell line's day 1 measurement ($n \geq 6$, $^{**}P \leq .01$, 2-way ANOVA followed by Bonferroni multiple comparison test, two independent experiments were performed).

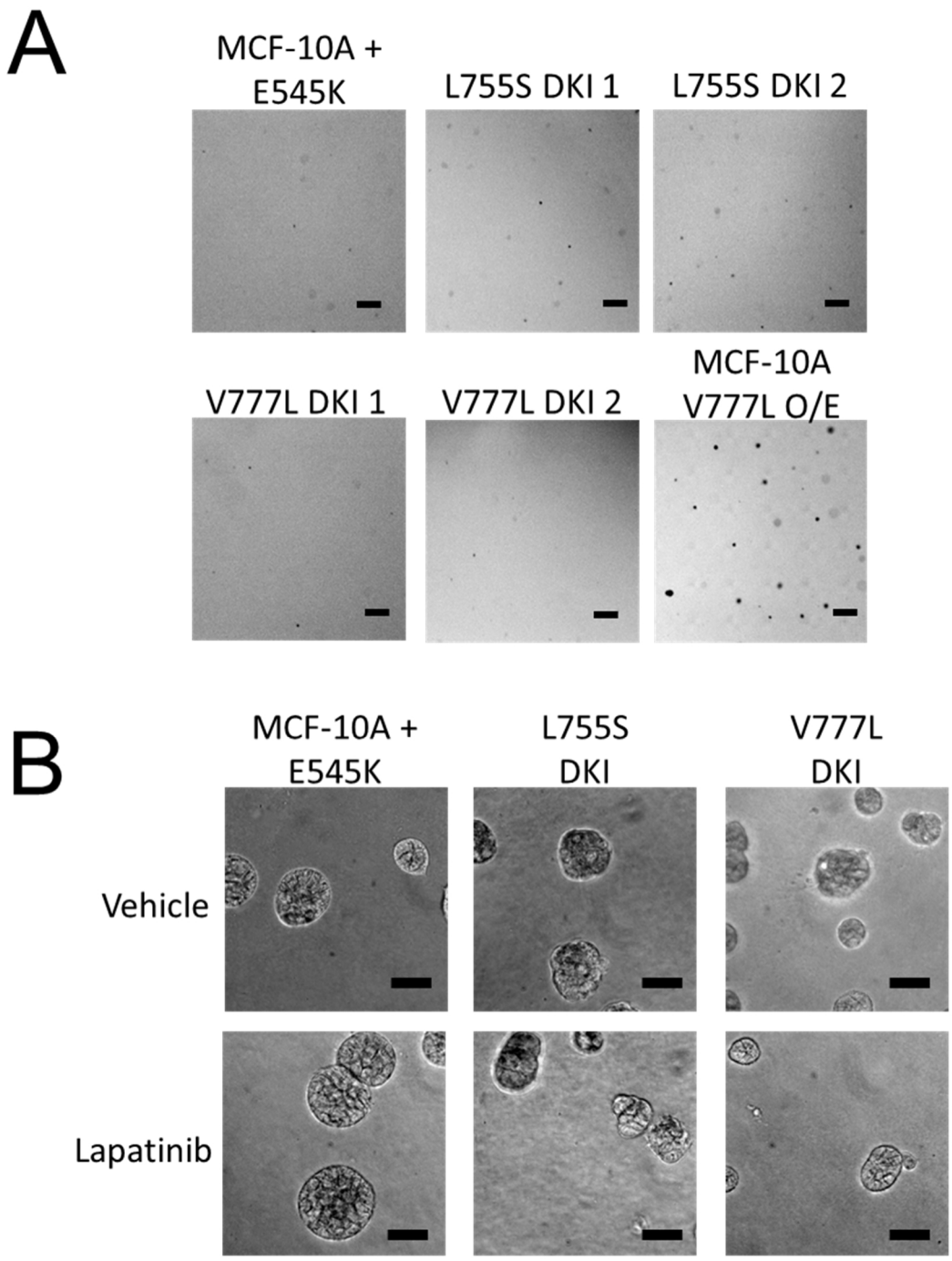

Figure 16: A) Representative images depicting soft agar colony formation in MCF-10A + E545K, L755S DKI, V777L DKI, and MCF-10A V777L overexpression cell lines after 4 weeks of incubation. Bar = 200μm. B) MCF-10A + E545K, L755S DKI, and V777L DKI cells were seeded into 3D Matrigel culture in the presence of DMSO vehicle or lapatinib (1μM) and photographed on day 12. Bar = 100μm.

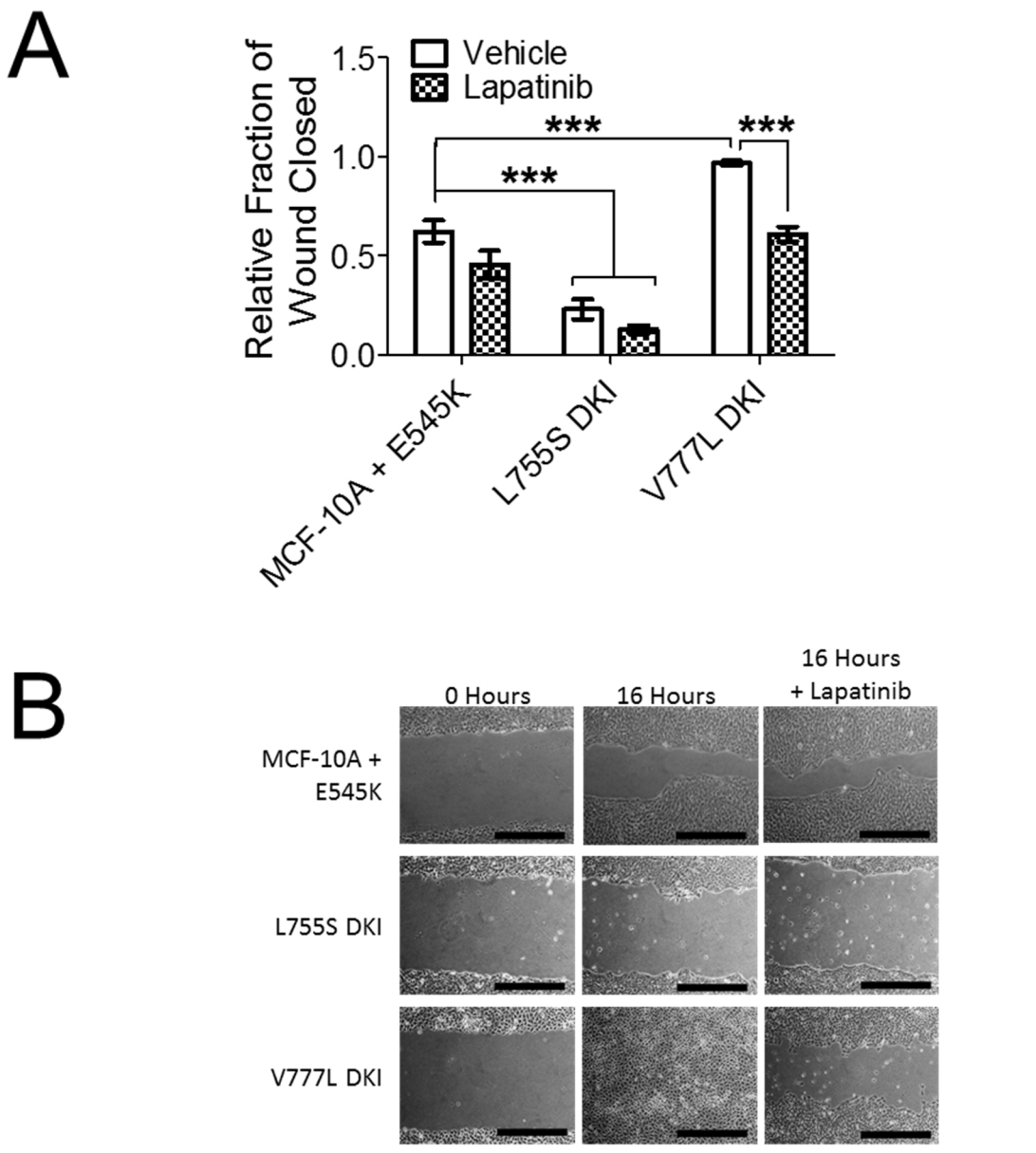

Figure 17: A) Relative fraction of scratch wound closure (±SEM) as measured after 16 hours. Cells were grown to near confluent monolayers, a wound was introduced, and assay media without EGF ± lapatinib (1μM) was added back to wells ($n \geq 14$, at least three independent experiments were performed, ***$P \leq .001$, 1-way ANOVA followed by Bonferroni multiple comparison test). B) Representative phase contrast images of wound closure. Bar = 500μm.

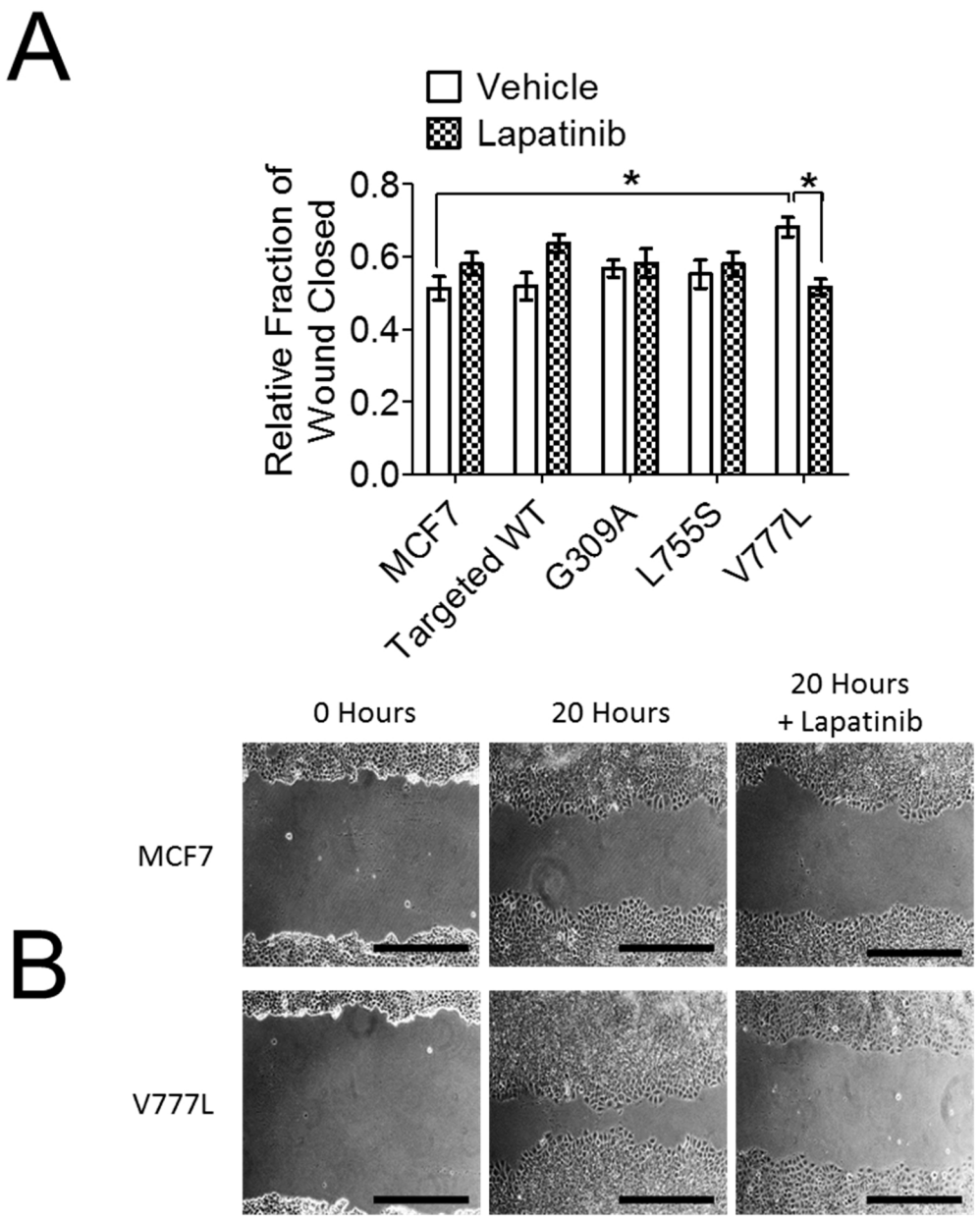

Figure 18: A) Relative fraction of scratch wound closure (±SEM) for MCF7 and *HER2* mutant derivatives in serum supplemented media ± lapatinib (5μM) after 20 hours ($n \geq 12$, $^*P \leq .05$, at least two independent experiments were performed, 1-way ANOVA followed by Bonferroni multiple comparison test). B) Representative images from MCF7 cell line scratch wound closure experiments. Bar = 500μm.

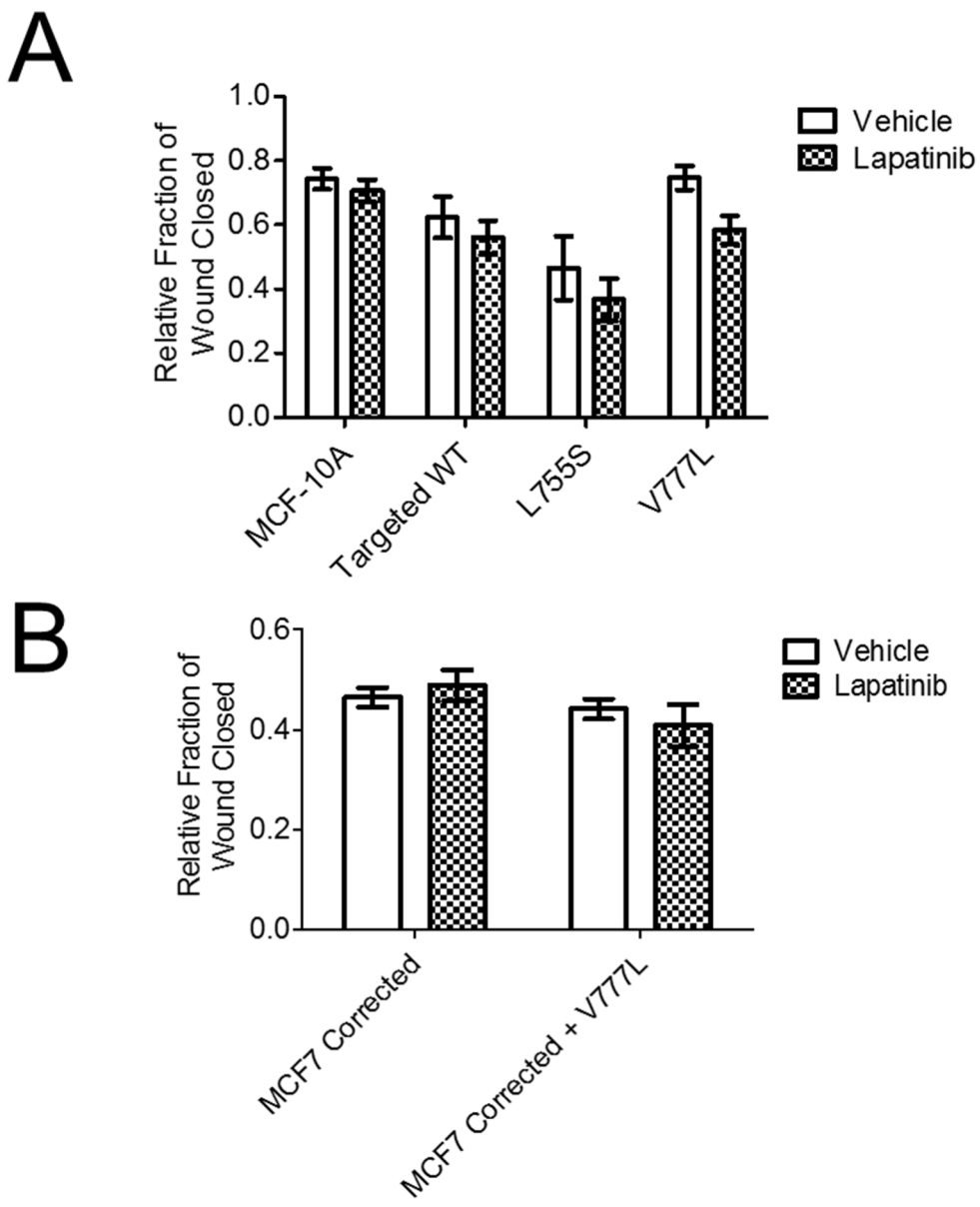

Figure 19: A) Mean (±SEM) relative fraction of scratch wound closure as measured after 16 hours for MCF-10A *HER2* mutant cells and controls ($n \geq 6$, at least two independent experiments were performed, $^*P \leq .05$, 1-way ANOVA followed by Bonferroni multiple comparison test). Cells were grown to confluent monolayers, a wound was introduced, and media with 20ng/mL EGF ± lapatinib (1μM) was added to the wells. B) Mean (±SEM) relative fraction of scratch wound closure after 20 hours for MCF7 corrected V777L mutants and controls in 10% serum supplemented media ± lapatinib (5μM) ($n \geq 10$, at least two independent experiments were performed).

A

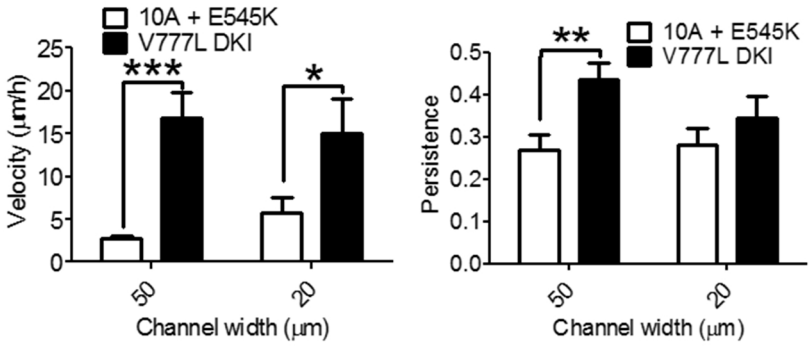

B

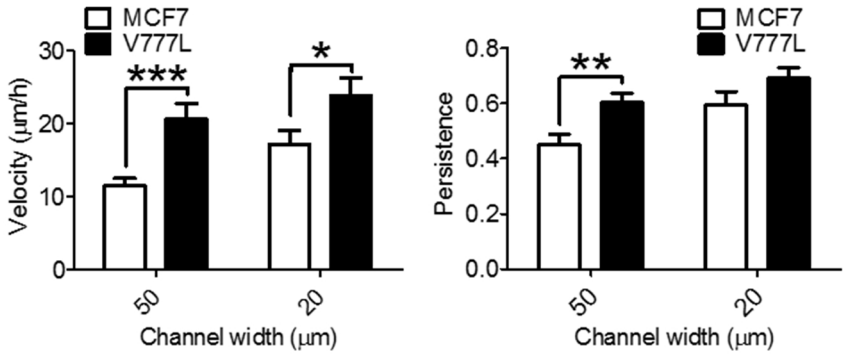

Figure 20: A) Mean (±SEM) cellular velocity (left) and persistence (net cellular displacement to total distance traveled ratio) (right) in microchannels for microchannel migration experiments of MCF-10A + E545K and V777L double knock in cell lines and MCF7 and MCF7 V777L cell lines (B) ($n \geq 30$ tracked cells, at least three independent experiments were performed, ***$P \leq .001$, **$P \leq .01$, *$P \leq .05$, unpaired T-test).

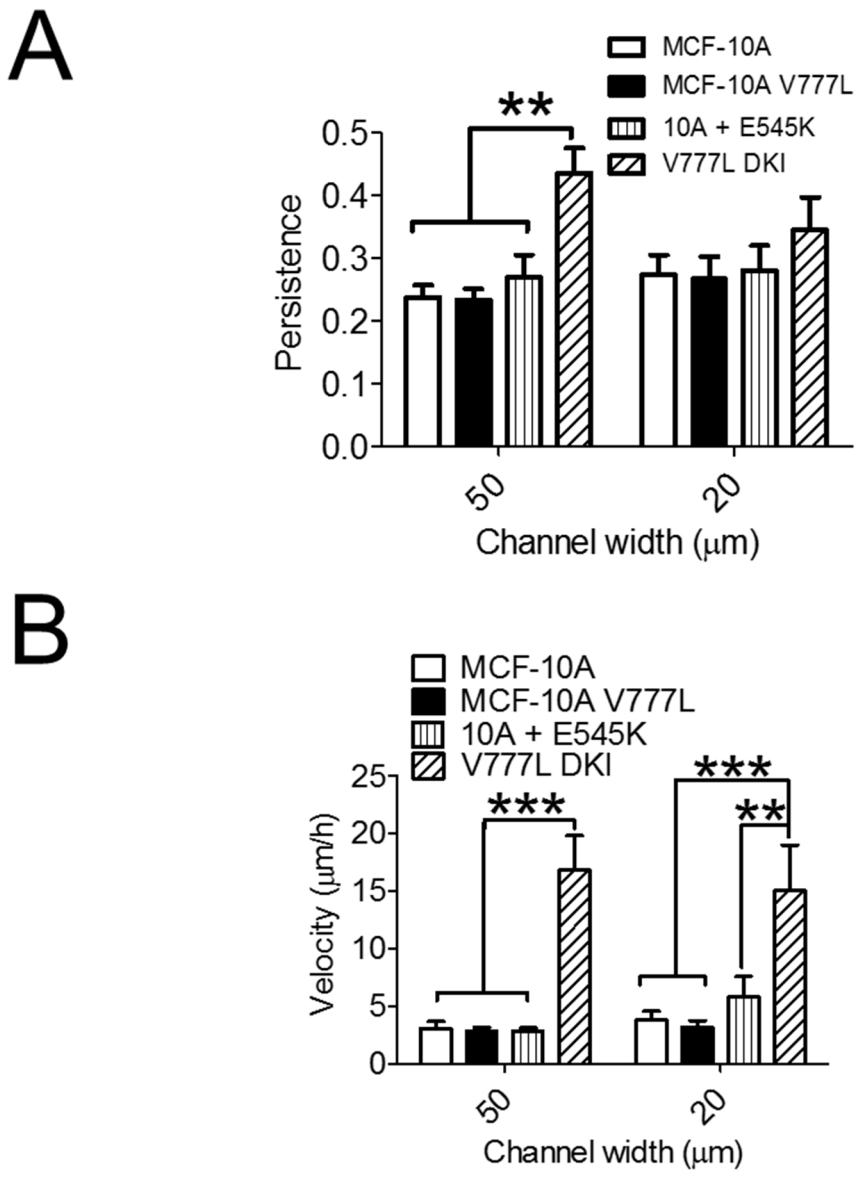

Figure 21: A) Mean (±SEM) persistence (net cell displacement to total distance traveled) in microchannels (left) and cellular velocity in microchannels (right) for microchannel migration experiments of MCF-10A parental, MCF-10A V777L, MCF-10A + E545K and V777L DKI cell lines ($n \geq 30$ tracked cells from at least three independent experiments, $^{**}P \leq .01$, $^{**}P \leq .001$, unpaired T-test).

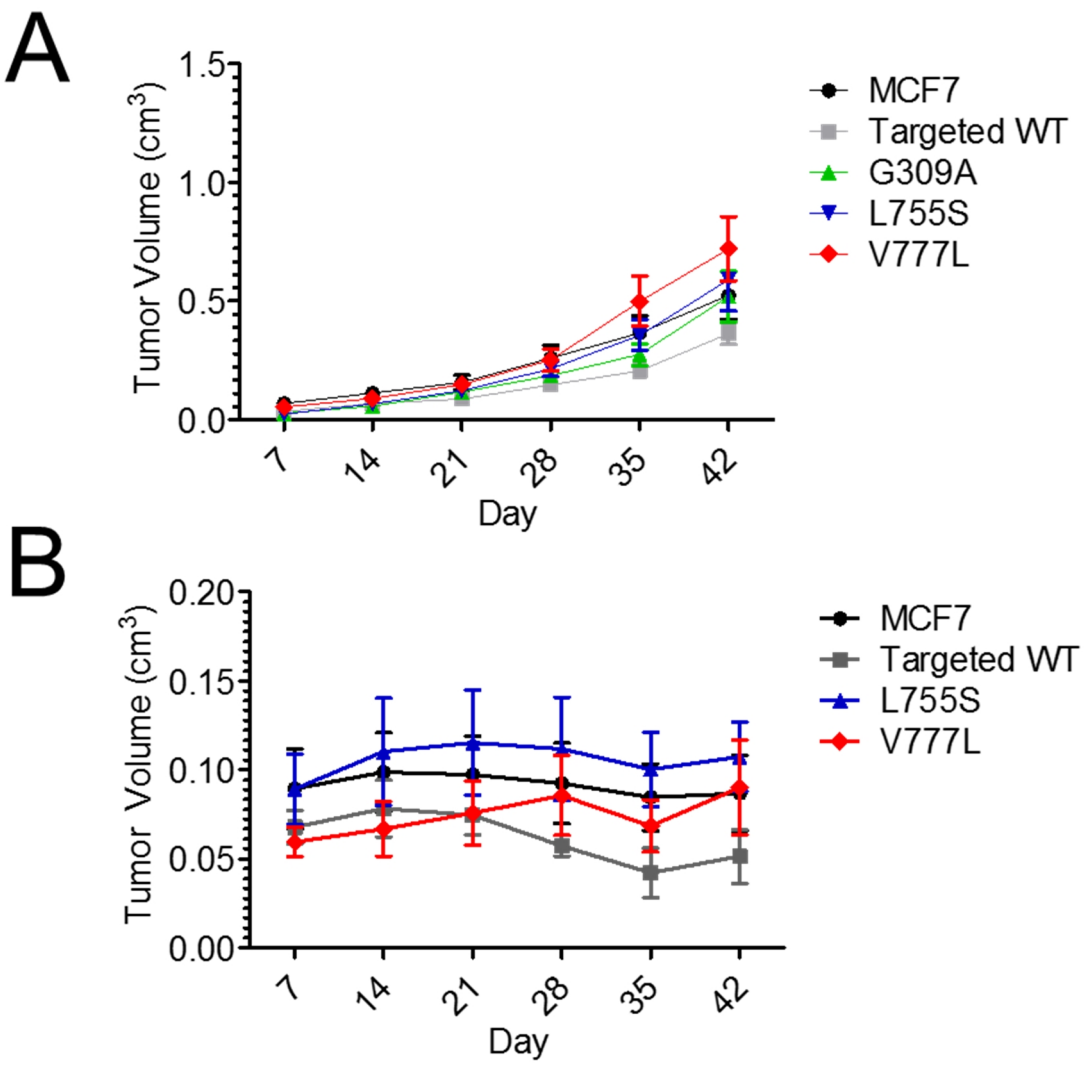

Figure 22: A) Mean (±SEM) *in vivo* tumor growth of MCF7 *HER2* mutants in mice supplemented with estrogen pellets. B) Mean (±SEM) *in vivo* tumor growth for MCF7 *HER2* mutants in mice without estrogen pellet supplementation. $n \geq 5$ animals per group (A-B).

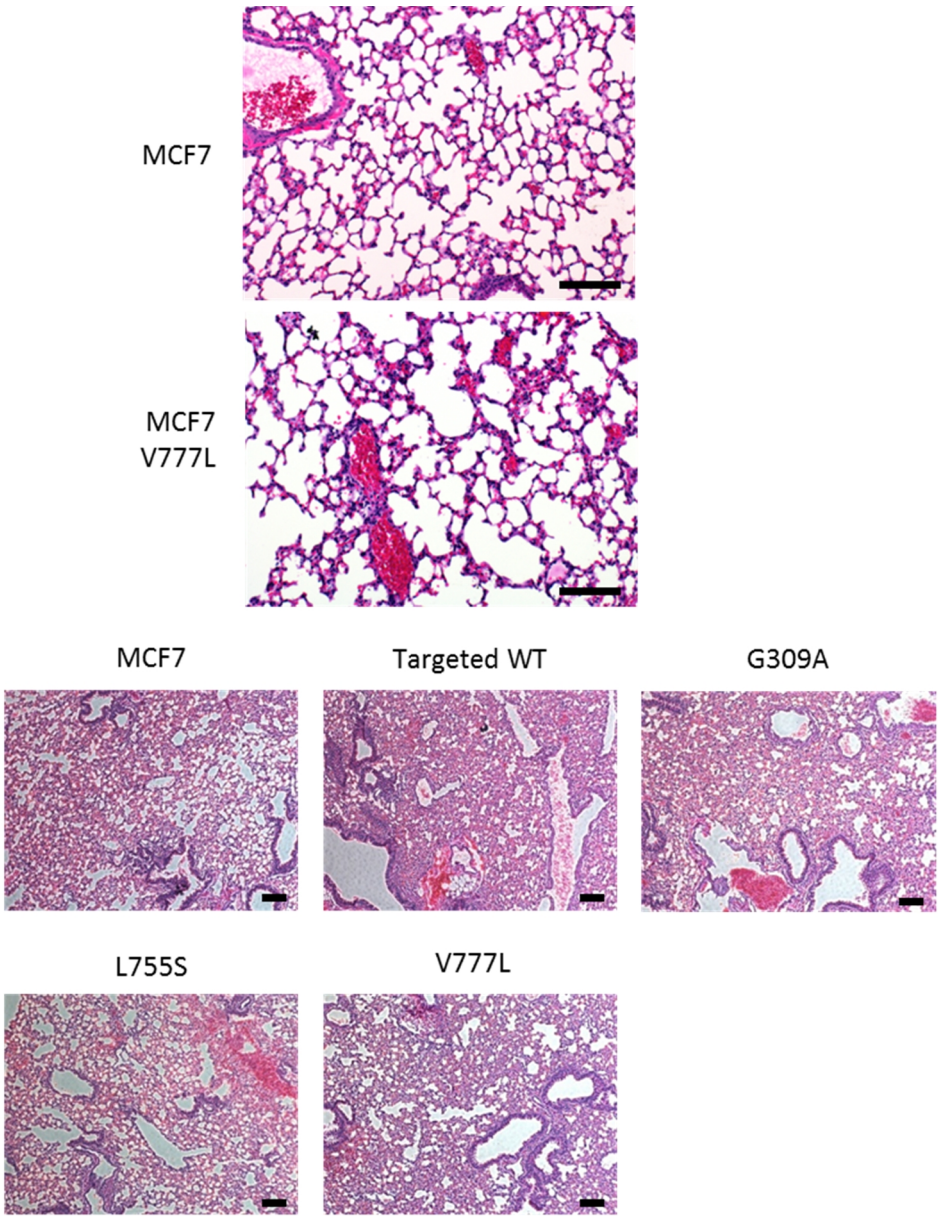

Figure 23: Representative images of H&E stained lung sections from tail vein injection assays showing benign lung parenchyma and lack of proliferating, multicellular sites of carcinoma. $n \geq 5$ animals per group. Bar = 100µm.

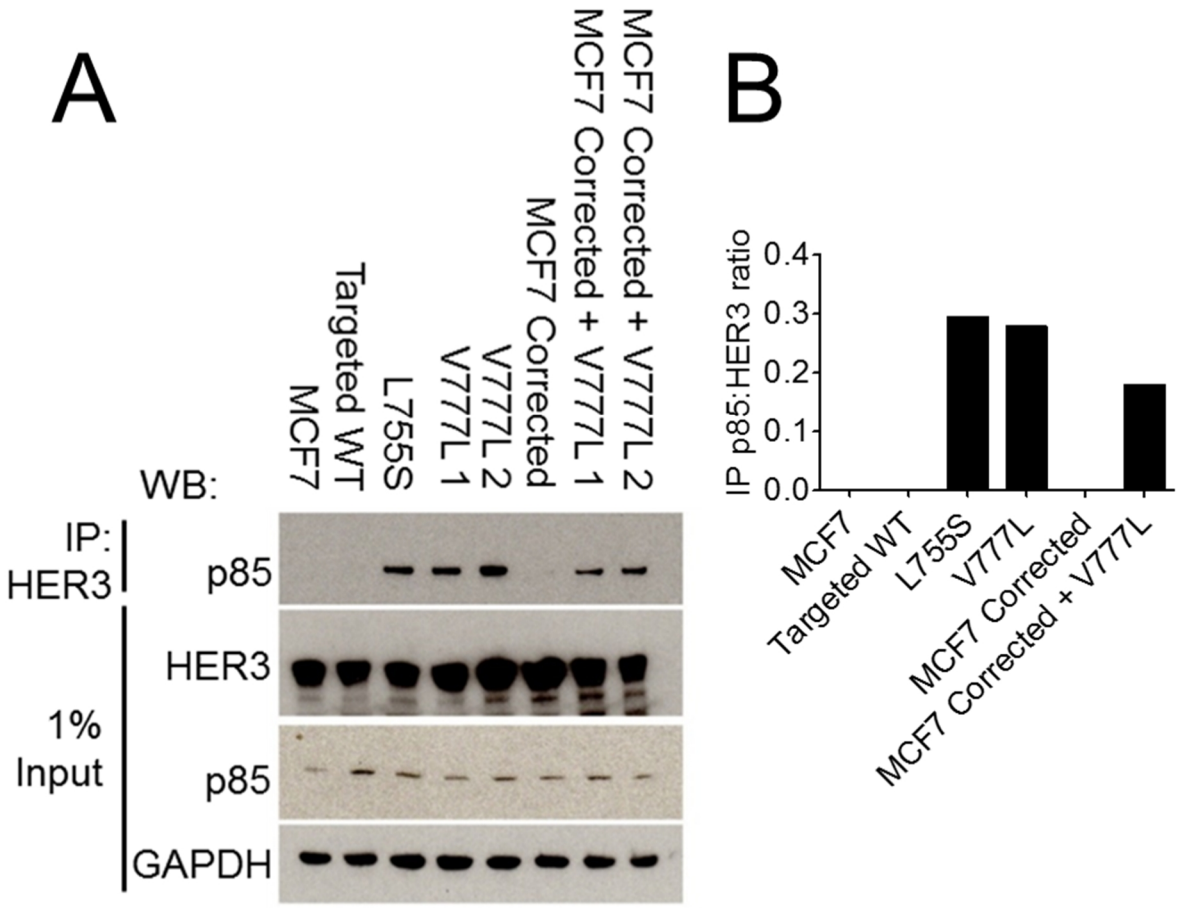

Figure 24: A) MCF7 parental, MCF7 corrected, and *HER2* mutant cell lysates were immunoprecipitated with a HER3 antibody. Antibody pulldowns were then subjected to western blotting analysis with the indicated primary antibodies. 1% of total protein was used as a control. B) Ratio of p85 after immunoprecipitation to HER3 input control western blot band as measured with ImageJ software. Bars for MCF7 V777L and MCF7 corrected + V777L represent the average of two clones.

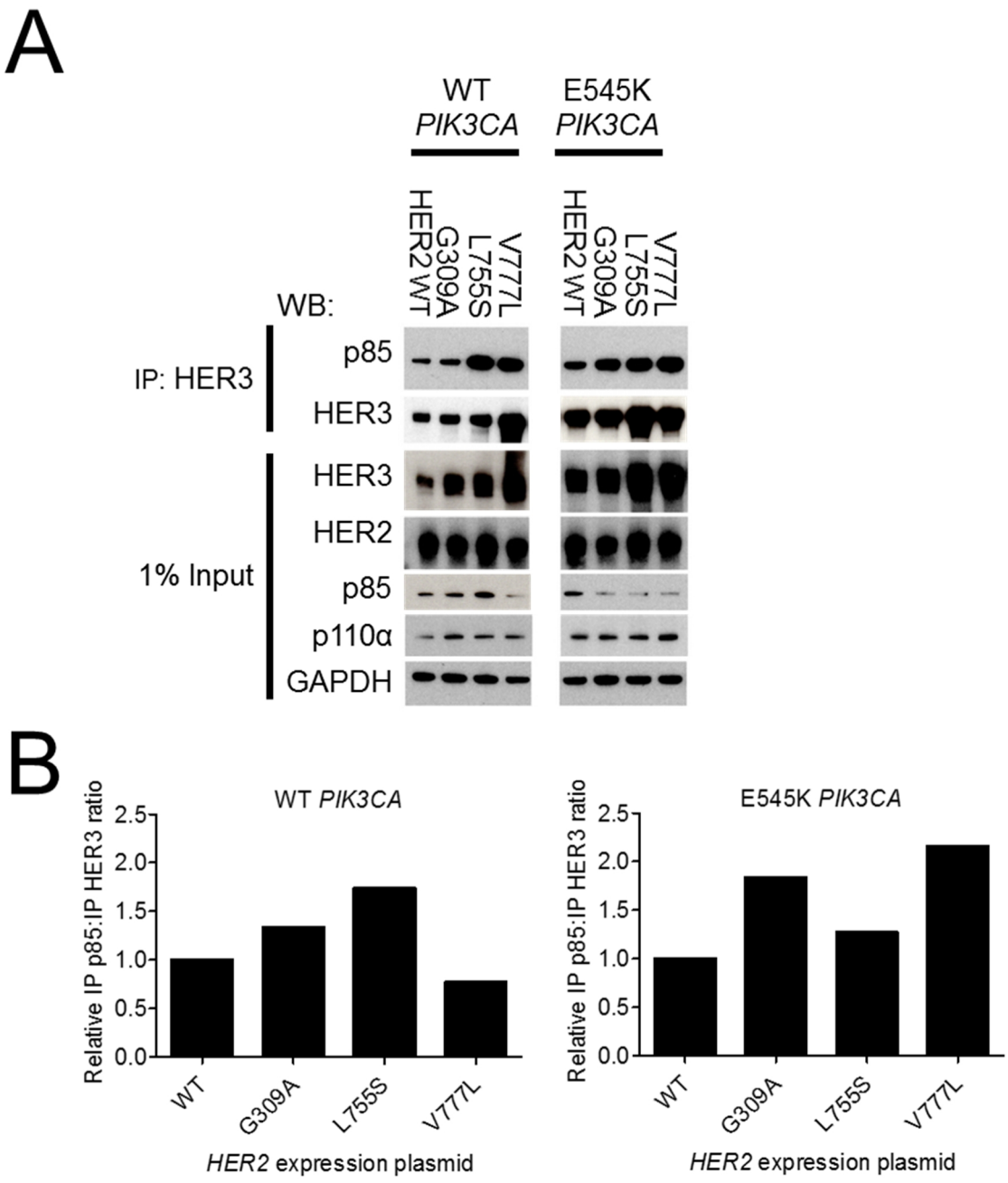

Figure 25: A) HEK293T cells were transfected with a HER3 overexpression plasmid and with the indicated *PIK3CA* and *HER2* overexpression plasmids. Lysates were immunprecipitated with a HER3 antibody and subjected to western blotting analysis with the indicated primary antibodies. 1% of total protein immunoprecipitated was immunoblotted as a control. B) Ratio of p85 to HER3 western blot band quantification after immunoprecipitation relative to wild type HER2 overexpression for wild type (left) or E545K (right) *PIK3CA* overexpression plasmids in HEK293T cells as measured with ImageJ software.

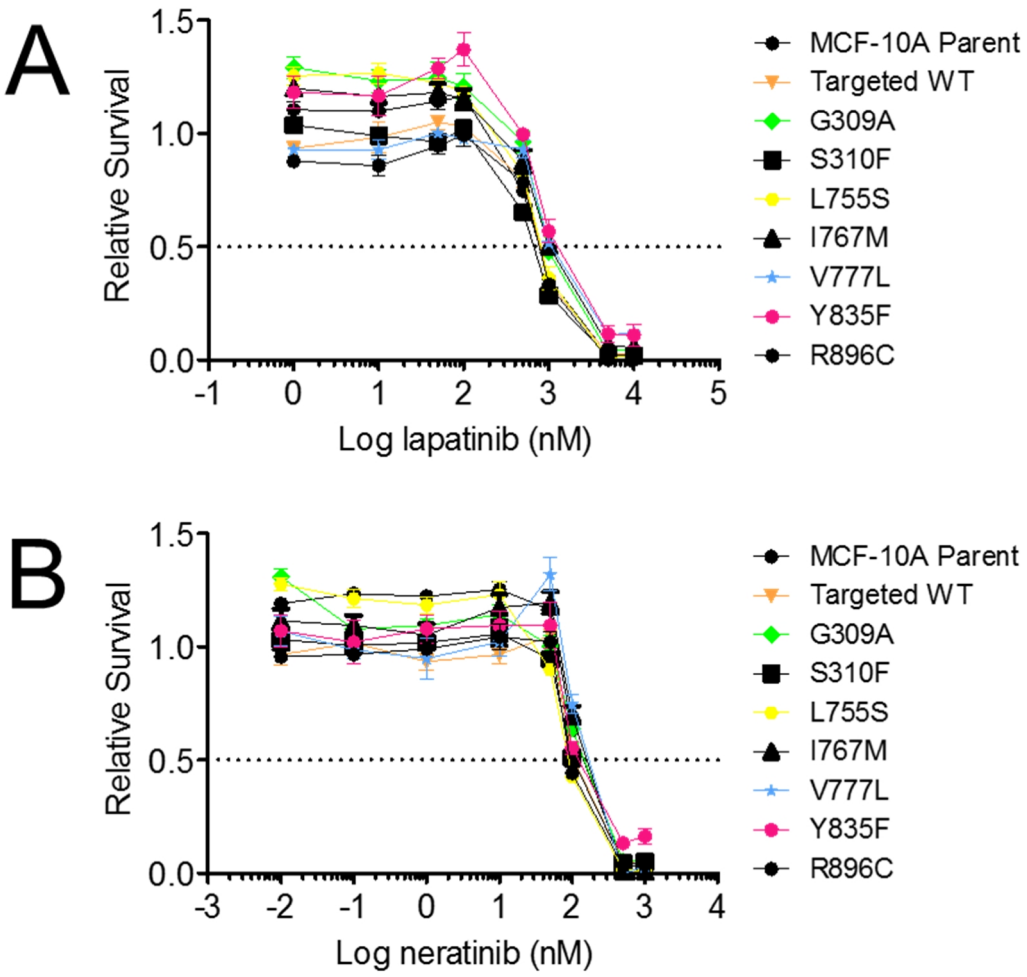

Figure 26: Dose inhibition curves for MCF-10A and MCF-10A *HER2* knock in cell lines for lapatinib (A) and neratinib (B) in assay media supplemented with 20ng/mL EGF.

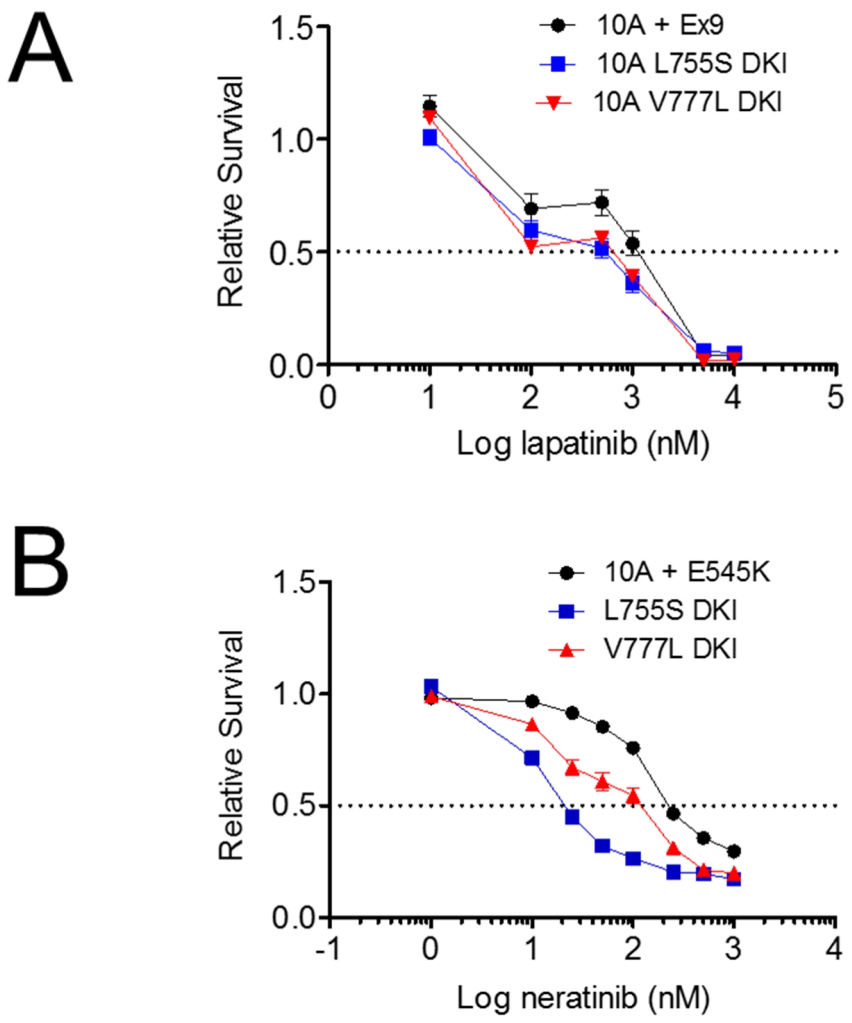

Figure 27: Dose inhibition curves for MCF-10A + E545K, L755S DKI, and V777L DKI cells treated with lapatinib (A) and neratinib (B) in assay media without EGF.

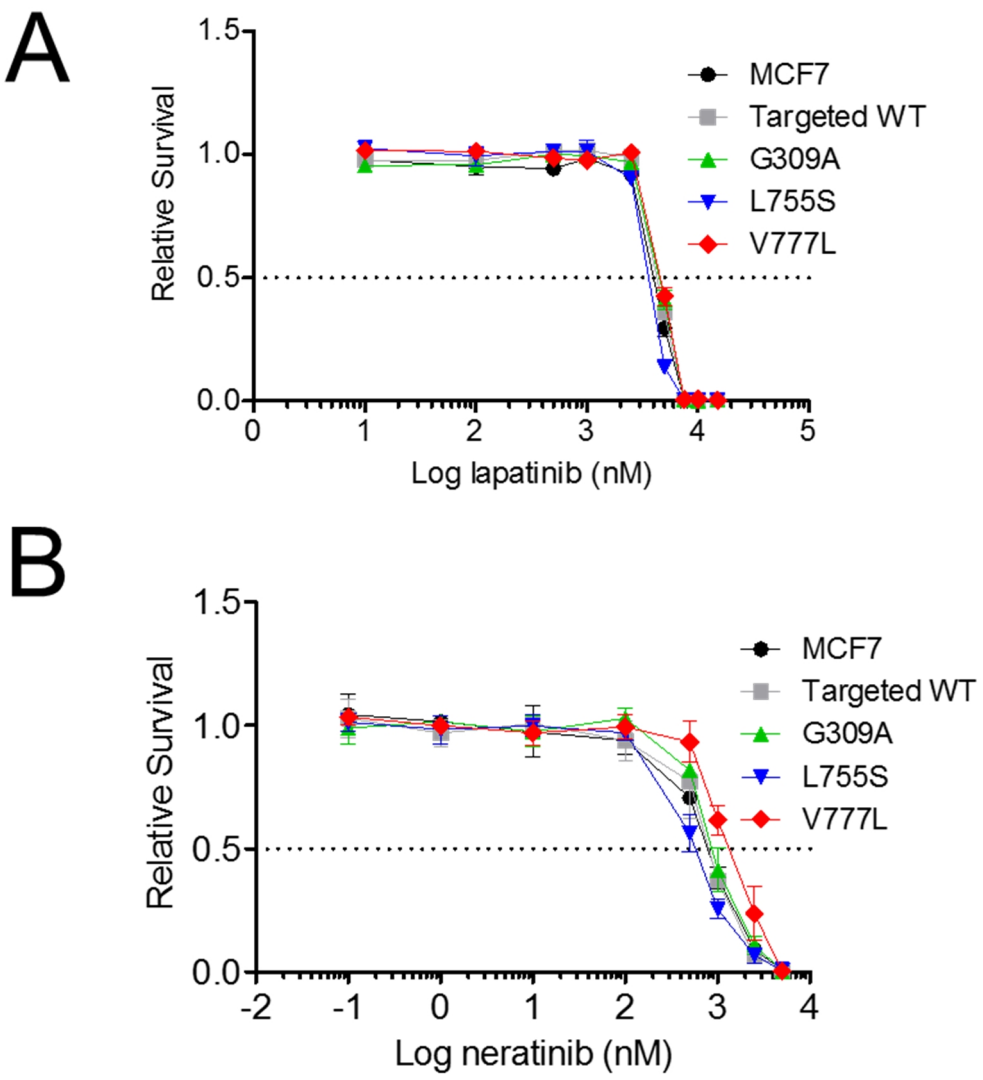

Figure 28: Dose inhibition curves for MCF7 derivatives treated with lapatinib (A) or neratinib (B) in serum supplemented media.

A

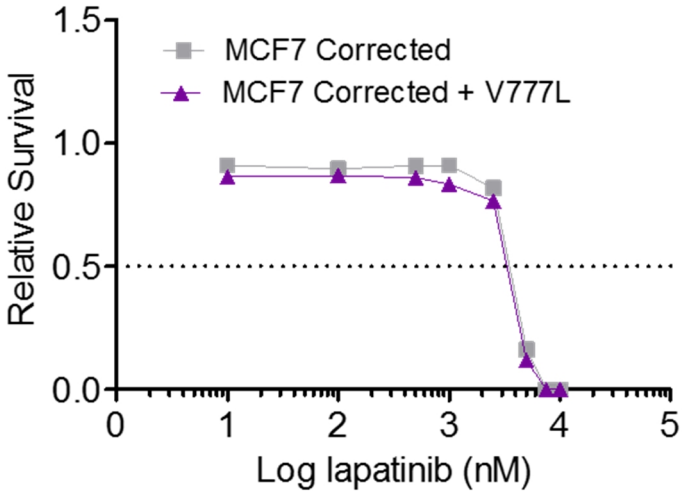

B

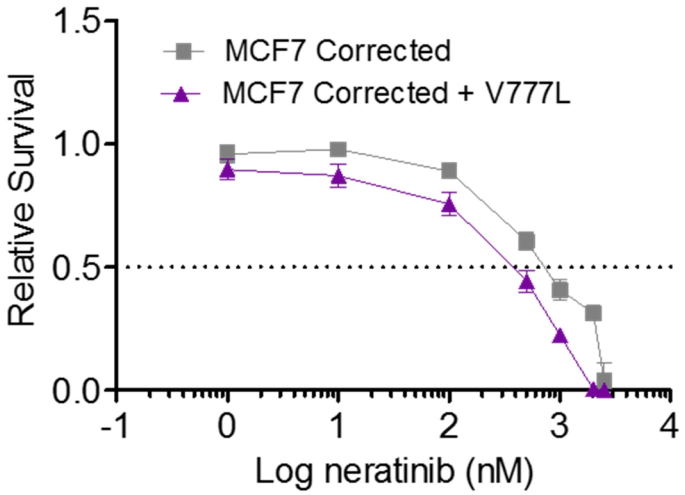

Figure 29: Dose inhibition curves for MCF7 corrected and MCF7 corrected + V777L cells treated with lapatinib (A) or neratinib (B) in serum supplemented media.

A

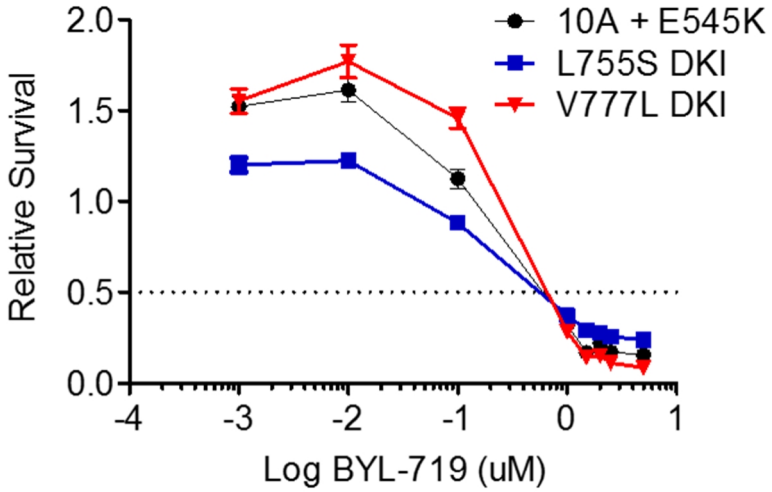

B

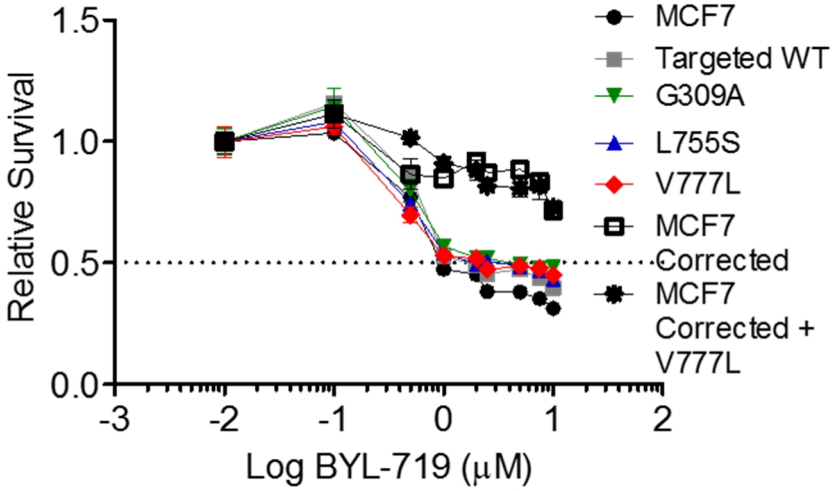

Figure 30: Dose inhibition curves for MCF-10A + E545K, L755S DKI, and V777L DKI treated with BYL-719 in assay media without EGF (A) and MCF7 derivatives and MCF7 corrected derivatives treated with BYL-719 in serum supplemented media (B).

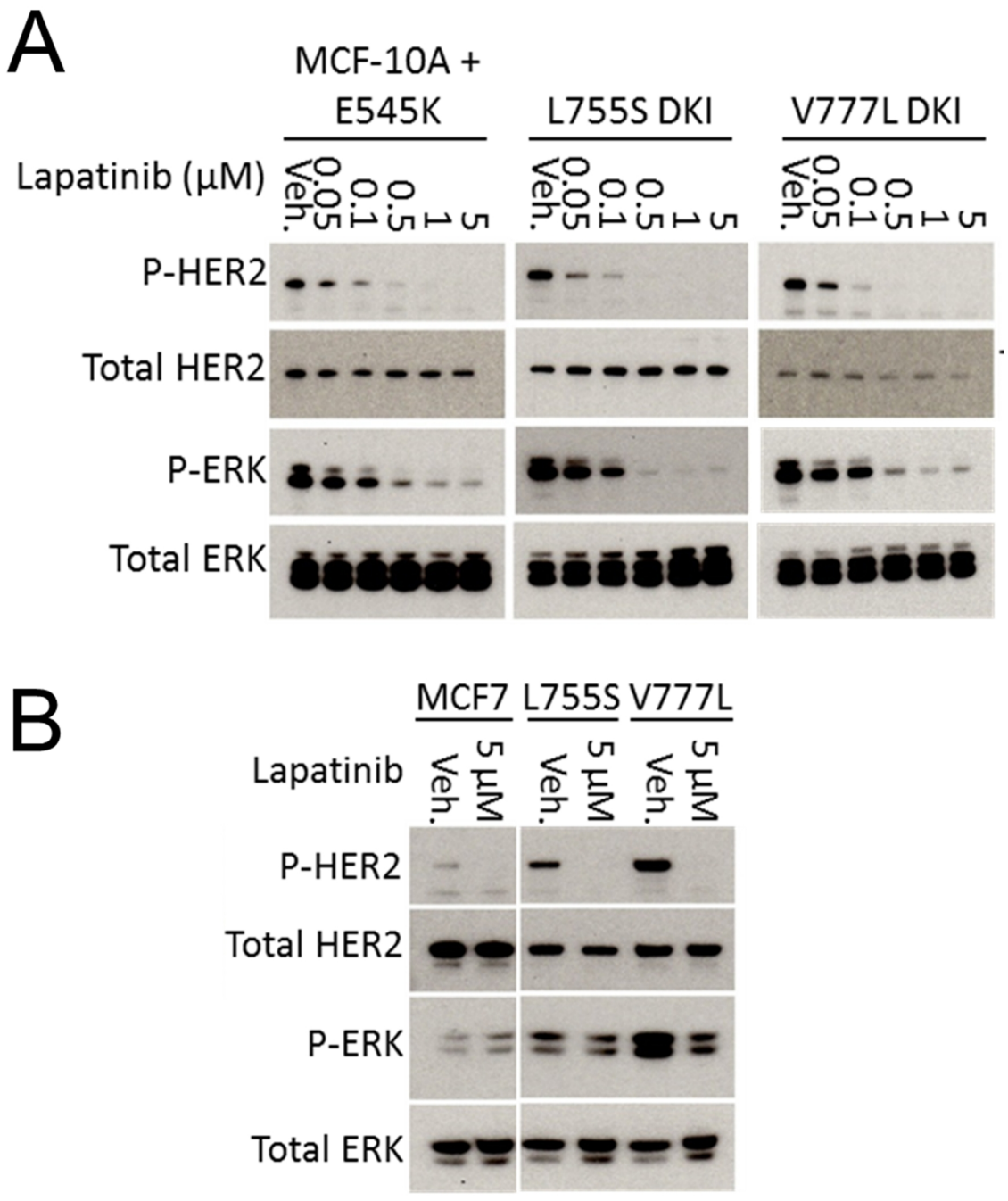

Figure 31: A) Effect of four hour lapatinib exposure for MCF-10A + E545K, L755S DKI, and V777L DKI cells in assay media supplemented with 0.2ng/mL EGF. B) Western blotting analysis for MCF7 parental, L755S, and V777L cells in serum starved media conditions after exposure to lapatinib for four hours. White line indicates that lanes have been cropped from the final image.

4 Discussion

HER2 mutations in non-amplified/non-overexpressed breast cancers represent a phenomenon that can potentially be exploited therapeutically. While previous overexpression studies of mutant *HER2* cDNAs have suggested that a number of *HER2* mutations are activating and promote transformation, our study found only the V777L mutation to be of functional significance. Perhaps most interesting, the effects of the *HER2* V777L mutation appear to be accentuated by a cooperating mutation, in this case the *PIK3CA* E545K hotspot mutation. Consistently across two different human breast cell line models, *HER2* V777L combined with *PIK3CA* E545K imparted features of increased signaling pathway activation and migration as noted by changes in western blotting, scratch wound healing, and microchannel migration assays. Notably, the *HER2* V777L kinase domain mutation led to an increased interaction between p85 and HER3 in the presence of a *PIK3CA* E545K mutation. These results suggest that HER2 missense mutations require additional genetic alterations to promote features of transformation. In addition, the HER2 mutation L755S, which previous

overexpression studies have shown imparts resistance to lapatinib (10,33,34,58) did not show obvious resistance phenotypes in our genome edited cell lines. It is conceivable that endogenous expression of L755S mutant HER2 in our models may not be sufficient to produce resistance to lapatinib due to lower levels of the mutant protein. This finding may be of clinical importance, since patients that do not have amplification/overexpression or high expression of L755S mutant *HER2* may still be sensitive to lapatinib, an FDA approved therapy for HER2-amplified breast cancers.

Targeting *HER2* mutations in *HER2* negative disease is a potential avenue to apply already FDA approved therapies to a new patient population. Indeed, trials are ongoing to test this hypothesis, but given the rarity and variety of *HER2* mutations, such trials may be underpowered to definitively address this question. Since the majority of *HER2* mutations in clinical samples are not amplified or overexpressed, we evaluated seven previously reported *HER2* mutations using somatic cell gene targeting to gain insight into this issue. However, we recognize that our models are limited in complexity compared to what is present in patients' tumors, where interacting factors including the immune system, varying protein expression levels, and tumor microenvironment can influence response to targeted therapies. Nonetheless, our isogenic cell line models of *HER2* mutations provide useful tools for understanding the functional consequences of *HER2* mutations in isolation and in combination with other oncogenes, as well as testing responses to targeted therapies.

Our study illustrates that different *HER2* mutations impart distinct or absent phenotypes depending on the individual mutation and the presence of other genetic alterations in oncogenes. This is perhaps not surprising given recent work demonstrating similar findings for *AKT1* and *HER3* mutations (59,60). This has implications for predicting response to targeted therapies. For example, in our study, *HER2* mutations did not overtly promote cell proliferation. Therefore it may be expected that HER2 targeted therapies would not show differential sensitivity to cells harboring these mutations in terms of reducing cell number in standard growth assays. On the other hand, the V777L *HER2* mutation in the appropriate context (e.g. oncogenic *PIK3CA* mutations) led to an increase in cellular migration, potentially resulting in increased metastatic potential that was affected by the HER2 inhibitor lapatinib. HER2-directed therapies in this regard may be capable of ablating this phenotype in patients, and therefore could possibly afford clinical benefit.

The variable effects of individual *HER2* mutations coupled with the requisite need for oncogene cooperativity may prove challenging for the use of *HER2* mutation status to guide therapy for breast cancer patients. Our studies have implicated oncogenic mutant *PIK3CA* as a potential partner to *HER2* mutations, and, indeed, *HER2* kinase domain mutations and *PIK3CA* mutations have been reported concurrently in breast cancer sequencing efforts (29). We tested the effects of *PIK3CA* mutations in conjunction with *HER2* mutations due to their close relationship as members of the same signaling pathway however, it is likely that there are other genes in the MAP Kinase and PI3 Kinase pathways,

which when mutated may cooperate with *HER2* missense mutations to impart transformative effects on cells. Indeed, the relatively low frequency of *HER2* missense mutations may be explained by a need for certain concurrent oncogenic mutations to achieve a selective advantage in *HER2* mutant tumors. Additionally, it may explain why many *HER2* mutations in our isogenic models did not have a detectable phenotype even though they are recurrently found in human cancers. Further work in this regard is ongoing and may help elucidate whether mechanisms of cooperativity are shared or unique among altered oncogenes and tumor suppressors and *HER2* mutations.

In conclusion, using an isogenic panel of non-amplified/non-overexpressed *HER2* mutant cell lines, we have determined that the majority of *HER2* mutations alone are not sufficient to promote transformative phenotypes in breast cell lines. However, *HER2* kinase domain mutations, notably V777L, can exhibit cooperativity with the activating *PIK3CA* E545K mutation. Cells with both *HER2* V777L and *PIK3CA* E545K mutations exhibited key features of transformation *in vitro*, including oncogenic signaling pathway activation and increased migratory potential, but not increased tumorigenicity *in vivo*. These findings provide new context for the study and clinical significance of *HER2* mutations, in that detailed analysis and study of co-existing mutations in patients may be required to make meaningful patient management decisions. For example, our results suggest that HER2-directed therapies such as lapatinib and neratinib may be effective in reducing cancer migration and not cell proliferation, but the context of cooperating oncogenic partners must be considered. Taken

together, our results have relevant translational implications, supporting that HER2 missense mutations are necessary but not sufficient for imparting features of a cancerous phenotype, and therefore may be targetable in the appropriate genetic context.

References

1. American Cancer Society. Breast Cancer Facts & Figures 2013-2014. American Cancer Society 2013.
2. Hanahan D, Weinberg RA. Hallmarks of cancer: the next generation. Cell 2011;144(5):646-74.
3. Sjöblom T, Jones S, Wood LD, Parsons DW, Lin J, Barber TD, et al. The consensus coding sequences of human breast and colorectal cancers. Science 2006;314(5797):268-74.
4. Wood LD, Parsons DW, Jones S, Lin J, Sjöblom T, Leary RJ, et al. The genomic landscapes of human breast and colorectal cancers. Science 2007;318(5853):1108-13.
5. Bachman KE, Argani P, Samuels Y, Silliman N, Ptak J, Szabo S, et al. The PIK3CA gene is mutated with high frequency in human breast cancers. Cancer Biol Ther 2004;3(8):772-5.
6. Weinstein IB. Cancer. Addiction to oncogenes--the Achilles heal of cancer. Science 2002;297(5578):63-4.
7. Yamamoto T, Saito M, Kumazawa K, Doi A, Matsui A, Takebe S, et al. ErbB2/HER2: Its Contribution to Basic Cancer Biology and the Development of Molecular Targeted Therapy. Breast Cancer - Carcinogenesis, Cell Growth and Signalling Pathways 2011.
8. Baselga J, Swain SM. Novel anticancer targets: revisiting ERBB2 and discovering ERBB3. Nat Rev Cancer 2009;9(7):463-75.

9. Ellis MJ, Ding L, Shen D, Luo J, Suman VJ, Wallis JW, et al. Whole-genome analysis informs breast cancer response to aromatase inhibition. Nature 2012;486(7403):353-60.
10. Bose R, Kavuri SM, Searleman AC, Shen W, Shen D, Koboldt DC, et al. Activating HER2 mutations in HER2 gene amplification negative breast cancer. Cancer discovery 2013;3(2):224-37.
11. Shah SP, Roth A, Goya R, Oloumi A, Ha G, Zhao Y, et al. The clonal and mutational evolution spectrum of primary triple-negative breast cancers. Nature 2012;486(7403):395-9.
12. Lee JW, Soung YH, Seo SH, Kim SY, Park CH, Wang YP, et al. Somatic mutations of ERBB2 kinase domain in gastric, colorectal, and breast carcinomas. Clin Cancer Res 2006;12(1):57-61.
13. Padhy LC, Shih C, Cowing D, Finkelstein R, Weinberg RA. Identification of a phosphoprotein specifically induced by the transforming DNA of rat neuroblastomas. Cell 1982;28(4):865-71.
14. Shih C, Padhy LC, Murray M, Weinberg RA. Transforming genes of carcinomas and neuroblastomas introduced into mouse fibroblasts. Nature 1981;290(5803):261-4.
15. Schechter AL, Stern DF, Vaidyanathan L, Decker SJ, Drebin JA, Greene MI, et al. The neu oncogene: an erb-B-related gene encoding a 185,000-Mr tumour antigen. Nature 1984;312(5994):513-6.

16. Downward J, Yarden Y, Mayes E, Scrace G, Totty N, Stockwell P, et al. Close similarity of epidermal growth factor receptor and v-erb-B oncogene protein sequences. Nature 1984;307(5951):521-7.

17. Schechter AL, Hung MC, Vaidyanathan L, Weinberg RA, Yang-Feng TL, Francke U, et al. The neu gene: an erbB-homologous gene distinct from and unlinked to the gene encoding the EGF receptor. Science 1985;229(4717):976-8.

18. Yarden Y, Sliwkowski MX. Untangling the ErbB signalling network. Nat Rev Mol Cell Biol 2001;2(2):127-37.

19. Herter-Sprie GS, Greulich H, Wong KK. Activating Mutations in ERBB2 and Their Impact on Diagnostics and Treatment. Frontiers in oncology 2013;3:86.

20. Arteaga CL, Engelman JA. ERBB receptors: from oncogene discovery to basic science to mechanism-based cancer therapeutics. Cancer Cell 2014;25(3):282-303.

21. Cho H-S, Mason K, Ramyar KX, Stanley AM, Gabelli SB, Denney DW, et al. Structure of the extracellular region of HER2 alone and in complex with the Herceptin Fab. Nature 2003;421(6924):756-60.

22. Garrett TPJ, McKern NM, Lou M, Elleman TC, Adams TE, Lovrecz GO, et al. The crystal structure of a truncated ErbB2 ectodomain reveals an active conformation, poised to interact with other ErbB receptors. Mol Cell 2003;11(2):495-505.

23. Hynes NE, Lane HA. ERBB receptors and cancer: the complexity of targeted inhibitors. Nat Rev Cancer 2005;5(5):341-54.

24. Aertgeerts K, Skene R, Yano J, Sang B-C, Zou H, Snell G, et al. Structural analysis of the mechanism of inhibition and allosteric activation of the kinase domain of HER2 protein. The Journal of biological chemistry 2011;286(21):18756-65.

25. Jura N, Shan Y, Cao X, Shaw DE, Kuriyan J. Structural analysis of the catalytically inactive kinase domain of the human EGF receptor 3. Proc Natl Acad Sci U S A 2009;106(51):21608-13.

26. Slamon DJ, Clark GM, Wong SG, Levin WJ, Ullrich A, McGuire WL. Human breast cancer: correlation of relapse and survival with amplification of the HER-2/neu oncogene. Science 1987;235(4785):177-82.

27. Moody SE, Sarkisian CJ, Hahn KT, Gunther EJ, Pickup S, Dugan KD, et al. Conditional activation of Neu in the mammary epithelium of transgenic mice results in reversible pulmonary metastasis. Cancer Cell 2002;2(6):451-61.

28. Geyer CE, Forster J, Lindquist D, Chan S, Romieu CG, Pienkowski T, et al. Lapatinib plus capecitabine for HER2-positive advanced breast cancer. N Engl J Med 2006;355(26):2733-43.

29. Cancer Genome Atlas Network. Comprehensive molecular portraits of human breast tumours. Nature 2012;490(7418):61-70.

30. Greulich H, Kaplan B, Mertins P, Chen TH, Tanaka KE, Yun CH, et al. Functional analysis of receptor tyrosine kinase mutations in lung cancer

identifies oncogenic extracellular domain mutations of ERBB2. Proc Natl Acad Sci U S A 2012;109(36):14476-81.

31. Rexer BN, Ghosh R, Narasanna A, Estrada MV, Chakrabarty A, Song Y, et al. Human breast cancer cells harboring a gatekeeper T798M mutation in HER2 overexpress EGFR ligands and are sensitive to dual inhibition of EGFR and HER2. Clin Cancer Res 2013;19(19):5390-401.

32. Wang SE, Narasanna A, Perez-Torres M, Xiang B, Wu FY, Yang S, et al. HER2 kinase domain mutation results in constitutive phosphorylation and activation of HER2 and EGFR and resistance to EGFR tyrosine kinase inhibitors. Cancer Cell 2006;10(1):25-38.

33. Trowe T, Boukouvala S, Calkins K, Cutler RE, Fong R, Funke R, et al. EXEL-7647 inhibits mutant forms of ErbB2 associated with lapatinib resistance and neoplastic transformation. Clin Cancer Res 2008;14(8):2465-75.

34. Kancha RK, von Bubnoff N, Bartosch N, Peschel C, Engh RA, Duyster J. Differential sensitivity of ERBB2 kinase domain mutations towards lapatinib. PLoS One 2011;6(10):e26760.

35. Konishi H, Karakas B, Abukhdeir AM, Lauring J, Gustin JP, Garay JP, et al. Knock-in of mutant K-ras in nontumorigenic human epithelial cells as a new model for studying K-ras mediated transformation. Cancer research 2007;67(18):8460-7.

36. Lauring J, Cosgrove DP, Fontana S, Gustin JP, Konishi H, Abukhdeir AM, et al. Knock in of the AKT1 E17K mutation in human breast epithelial cells

does not recapitulate oncogenic PIK3CA mutations. Oncogene 2010;29(16):2337-45.

37. Di Nicolantonio F, Arena S, Gallicchio M, Zecchin D, Martini M, Flonta SE, et al. Replacement of normal with mutant alleles in the genome of normal human cells unveils mutation-specific drug responses. Proc Natl Acad Sci U S A 2008;105(52):20864-9.

38. Wang GM, Wong HY, Konishi H, Blair BG, Abukhdeir AM, Gustin JP, et al. Single copies of mutant KRAS and mutant PIK3CA cooperate in immortalized human epithelial cells to induce tumor formation. Cancer research 2013;73(11):3248-61.

39. Gustin JP, Karakas B, Weiss MB, Abukhdeir AM, Lauring J, Garay JP, et al. Knockin of mutant PIK3CA activates multiple oncogenic pathways. Proc Natl Acad Sci U S A 2009;106(8):2835-40.

40. Beaver JA, Gustin JP, Yi KH, Rajpurohit A, Thomas M, Gilbert SF, et al. PIK3CA and AKT1 mutations have distinct effects on sensitivity to targeted pathway inhibitors in an isogenic luminal breast cancer model system. Clin Cancer Res 2013;19(19):5413-22.

41. Topaloglu O, Hurley PJ, Yildirim O, Civin CI, Bunz F. Improved methods for the generation of human gene knockout and knockin cell lines. Nucleic Acids Res 2005;33(18):e158.

42. Ho SN, Hunt HD, Horton RM, Pullen JK, Pease LR. Site-directed mutagenesis by overlap extension using the polymerase chain reaction. Gene 1989;77(1):51-9.

43. Konishi H, Lauring J, Garay JP, Karakas B, Abukhdeir AM, Gustin JP, et al. A PCR-based high-throughput screen with multiround sample pooling: application to somatic cell gene targeting. Nat Protoc 2007;2(11):2865-74.
44. Debnath J, Muthuswamy SK, Brugge JS. Morphogenesis and oncogenesis of MCF-10A mammary epithelial acini grown in three-dimensional basement membrane cultures. Methods 2003;30(3):256-68.
45. Balzer EM, Tong Z, Paul CD, Hung W-C, Stroka KM, Boggs AE, et al. Physical confinement alters tumor cell adhesion and migration phenotypes. FASEB J 2012;26(10):4045-56.
46. Tong Z, Balzer EM, Dallas MR, Hung W-C, Stebe KJ, Konstantopoulos K. Chemotaxis of cell populations through confined spaces at single-cell resolution. PLoS One 2012;7(1):e29211.
47. Hung W-C, Chen S-H, Paul CD, Stroka KM, Lo Y-C, Yang JT, et al. Distinct signaling mechanisms regulate migration in unconfined versus confined spaces. J Cell Biol 2013;202(5):807-24.
48. Stroka KM, Konstantopoulos K. Physical biology in cancer. 4. Physical cues guide tumor cell adhesion and migration. American journal of physiology Cell physiology 2014;306(2):C98-c109.
49. Subik K, Lee J-F, Baxter L, Strzepek T, Costello D, Crowley P, et al. The Expression Patterns of ER, PR, HER2, CK5/6, EGFR, Ki-67 and AR by Immunohistochemical Analysis in Breast Cancer Cell Lines. Breast Cancer (Auckl) 2010;4:35-41.

50. Soule HD, Maloney TM, Wolman SR, Peterson WD, Jr., Brenz R, McGrath CM, et al. Isolation and characterization of a spontaneously immortalized human breast epithelial cell line, MCF-10. Cancer research 1990;50(18):6075-86.

51. Gabelli SB, Echeverria I, Alexander M, Duong-Ly KC, Chaves-Moreira D, Brower ET, et al. Activation of PI3Kα by physiological effectors and by oncogenic mutations: structural and dynamic effects. Biophys Rev 2014;6(1):89-95.

52. Masuda H, Zhang D, Bartholomeusz C, Doihara H, Hortobagyi GN, Ueno NT. Role of epidermal growth factor receptor in breast cancer. Breast Cancer Res Treat 2012;136(2):331-45.

53. Hart JR, Zhang Y, Liao L, Ueno L, Du L, Jonkers M, et al. The butterfly effect in cancer: A single base mutation can remodel the cell. Proc Natl Acad Sci U S A 2015.

54. Li N, Jiang P, Du W, Wu Z, Li C, Qiao M, et al. Siva1 suppresses epithelial-mesenchymal transition and metastasis of tumor cells by inhibiting stathmin and stabilizing microtubules. Proc Natl Acad Sci U S A 2011;108(31):12851-6.

55. Barkan D, Kleinman H, Simmons JL, Asmussen H, Kamaraju AK, Hoenorhoff MJ, et al. Inhibition of metastatic outgrowth from single dormant tumor cells by targeting the cytoskeleton. Cancer research 2008;68(15):6241-50.

56. Chakrabarty A, Rexer BN, Wang SE, Cook RS, Engelman JA, Arteaga CL. H1047R phosphatidylinositol 3-kinase mutant enhances HER2-mediated transformation by heregulin production and activation of HER3. Oncogene 2010;29(37):5193-203.

57. Blair BG, Wu X, Zahari MS, Mohseni M, Cidado J, Wong HY, et al. A phosphoproteomic screen demonstrates differential dependence on HER3 for MAP kinase pathway activation by distinct PIK3CA mutations. Proteomics 2015;15(2-3):318-26.

58. Yang B, Zhang H, Wang H. Atomistic insights into the lung cancer-associated L755P mutation in HER2 resistance to lapatinib: a molecular dynamics study. J Mol Model 2015;21(2):2580.

59. Jaiswal BS, Kljavin NM, Stawiski EW, Chan E, Parikh C, Durinck S, et al. Oncogenic ERBB3 mutations in human cancers. Cancer Cell 2013;23(5):603-17.

60. Yi KH, Axtmayer J, Gustin JP, Rajpurohit A, Lauring J. Functional analysis of non-hotspot AKT1 mutants found in human breast cancers identifies novel driver mutations: implications for personalized medicine. Oncotarget 2013;4(1):29-34.

Curriculum Vitae

Daniel J. Zabransky

1650 Orleans Street, CRB 1 Room 116, Baltimore, MD 21287
703.895.5062 | dzabran1@jhmi.edu

Education

Cellular and Molecular Medicine Program
The Johns Hopkins University, Baltimore, MD
Thesis Advisor: Ben Ho Park, M.D., Ph.D.
Thesis Dissertation: "*HER2* missense mutations have distinct effects on oncogenic signaling and migration"

Bachelor of Science in Biology 2009
The College of William & Mary, Williamsburg, VA
summa cum laude

Research Experience

The Johns Hopkins University School of Medicine 2011-2015
Ph.D. Graduate Student, Park Laboratory Baltimore, MD
Utilized genome editing techniques to create a panel of isogenic cell lines carrying heterozygous *HER2* missense mutations. Characterized the biological implications of *HER2* missense mutations in *HER2* negative disease.

The Johns Hopkins University School of Medicine 2010-2011
Rotation Student, Drake Laboratory Baltimore, MD
Characterized the phenotypic and functional differences between Helios^{+} and Helios^{-} T-regulatory cells and their potential roles in the tumor microenvironment. Studied biochemical and immunologic changes that occur in men with prostate cancer after treatment lenalidomide.

The College of William & Mary 2008-2009
Undergraduate Research Student, Wawersik Laboratory Williamsburg, VA
Characterized localization and inheritance of centrosomes in the embryonic and larval stages of drosophila development using fluorescence microscopy.

National Cancer Institute, National Institutes of Health 2008
Summer Research Intern, Ped. Onc. Branch, Helman Laboratory Bethesda, MD
Characterized an osteosarcoma tumor subtype and determined it originates from neural precursor cells rather than mesenchymal cells. Used multiplex PCR to identify changes in gene signature that occur when EWS-FLI1 is overexpressed in non-cancerous cell lines. Created cell lines containing EWS-FLI1 driven luciferase reporters for using in a high-throughput drug screen for compounds that specifically inhibit EWS-FLI1 activity.

National Cancer Institute, National Institutes of Health 2006
Undergraduate Research Student, Subramaniam Laboratory Bethesda, MD

Modeled contact between HIV and T-cells and mapped spatial locations of bacterial chemotaxis receptors using cryo-electron tomography. Developed novel denoising algorithms for use with cryo-electron tomography data sets.

The College of William & Mary 2005-2006
Undergraduate Research Student, Cristol Laboratory Williamsburg, VA

Analyzed the effects of mercury contamination on birdsong in three different songbird species. Determined that birds living in areas with high levels of mercury contamination had lower reproductive fitness compared to birds living in uncontaminated reference areas.

Grants

- Howard Hughes Medical Institute Freshman Research Program, January 2006
- William & Mary Monroe Summer Grant, Summer 2006
- William & Mary Monroe Research Grant, Summer 2008
- NIH National Cancer Institute Cancer Research Training Grant: Summers 2006-2008

Honors & Awards

- 2009 William & Mary Cornell Pre-medical Student Award
- 2008 Barry M. Goldwater Scholarship recipient
- 2007 Barry M. Goldwater Scholarship Honorable Mention
- Monroe Scholar program at William & Mary, 2005-2009
- Dean's List, The College of William and Mary, Fall 2005-Spring 2009

Publications

Zabransky DJ, Yankaskas CL, Cochran RL, Wong HY, Croessmann S, Chu D, Kavuri SM, Red Brewer M, Rosen DM, Dalton WB, Cimino-Mathews A, Cravero K, Button B, Kyker-Snowman K, Cidado J, Erlanger B, Parsons H, Manto KM, Bose R, Lauring J, Arteaga CL, Konstantopoulos K, Park BH. *HER2* missense mutations have distinct effects on oncogenic signaling and migration. *In submission*.

Chu D, Paoletti C, Gersch C, VanDenBerg DA, **Zabransky DJ**, Cochran RL, Wong HY, Toro PV, Cidado J, Croessmann S, Erlanger B, Cravero K, Kyker-Snowman K, Button B, Parsons H, Dalton WB, Gillani R, Medford A, Aung K, Tokudome N, Chinnaiyan A, Schott A, Robertson D, Jacks KS, Lauring J, Hurley P, Hayes DF, Rae J, Park BH. ESR1 mutations in circulating plasma tumor DNA from metastatic breast cancer patients. *In submission*.

Croessmann S, Wong HY, **Zabransky DJ**, Chu D, Mendonca J, Sharma A, Mohseni M, Rosen DM, Scarpf R, Cidado J, Cochran RL, Parsons H, Dalton WB, Erlanger B, Button B, Cravero K, Kyker-Snowman K, Beaver JA, Kachhap S, Hurley PJ, Lauring J, Park

BH. NDRG1 links p53 with proliferation mediated centrosome homeostasis and genome stability. *In submission*.

Cochran RL, Cidado J, Kim M, **Zabransky DJ**, Croessmann S, Chu D, Wong HY, Beaver JA, Cravero K, Erlanger B, Parson H, Heaphy CM, Meeker AK, Lauring J, Park BH. Functional isogenic modeling of BRCA1 alleles reveals distinct carrier phenotypes. *In press at Oncotarget*.

Blair BG, Wu X, Zahari MS, Mohseni M, Cidado J, Wong HY, Beaver JA, Cochran RL, **Zabransky DJ**, Croessmann S, Chu D, Toro PV, Cravero K, Pandey A, Park BH. A phosphoproteomic screen demonstrates differential dependence on HER3 for MAP kinase pathway activation by distinct PIK3CA mutations. Proteomics. 2015 Jan;15(2-3):318-26. doi: 10.1002/pmic.201400342. Epub 2014 Dec 28. PubMed PMID: 25367220; PubMed Central PMCID: PMC4352327.

Mohseni M, Cidado J, Croessmann S, Cravero K, Cimino-Mathews A, Wong HY, Scharpf R, **Zabransky DJ**, Abukhdeir AM, Garay JP, Wang GM, Beaver JA, Cochran RL, Blair BG, Rosen DM, Erlanger B, Argani P, Hurley PJ, Lauring J, Park BH. MACROD2 overexpression mediates estrogen independent growth and tamoxifen resistance in breast cancers. Proc Natl Acad Sci U S A. 2014 Dec 9;111(49):17606-11. doi: 10.1073/pnas.1408650111. Epub 2014 Nov 24. PubMed PMID: 25422431; PubMed Central PMCID: PMC4267353.

Cochran RL, Cravero K, Chu D, Erlanger B, Toro PV, Beaver JA, **Zabransky DJ**, Wong HY, Cidado J, Croessmann S, Parsons HA, Kim M, Wheelan SJ, Argani P, Park BH. Analysis of BRCA2 loss of heterozygosity in tumor tissue using droplet digital polymerase chain reaction. Hum Pathol. 2014 Jul;45(7):1546-50. doi: 10.1016/j.humpath.2014.03.013. Epub 2014 Apr 13. PubMed PMID: 24824029; PubMed Central PMCID: PMC4065621.

Forde PM, Cochran RL, Boikos SA, **Zabransky DJ**, Beaver JA, Meyer CF, Thornton KA, Montgomery EA, Lidor AO, Donehower RC, Park BH. Familial GI Stromal Tumor With Loss of Heterozygosity and Amplification of Mutant KIT. J Clin Oncol. 2014 May 27. pii: JCO.2013.51.6633. [Epub ahead of print] PubMed PMID: 24868028.

Beaver JA, Jelovac D, Balukrishna S, Cochran RL, Croessmann S, **Zabransky DJ**, Wong HY, Valda Toro P, Cidado J, Blair BG, Chu D, Burns T, Higgins MJ, Stearns V, Jacobs L, Habibi M, Lange J, Hurley PJ, Lauring J, VanDenBerg DA, Kessler J, Jeter S, Samuels ML, Maar D, Cope L, Cimino-Mathews A, Argani P, Wolff AC, Park BH. Detection of cancer DNA in plasma of patients with early-stage breast cancer. Clin Cancer Res. 2014 May 15;20(10):2643-50. doi: 10.1158/1078-0432.CCR-13-2933. Epub 2014 Feb 6. PubMed PMID: 24504125; PubMed Central PMCID: PMC4024333.

Zabransky DJ, Smith HA, Thoburn CJ, Zahurak M, Keizman D, Carducci M, Eisenberger MA, McNeel DG, Drake CG, Antonarakis ES. Lenalidomide modulates IL-8 and anti-prostate antibody levels in men with biochemically recurrent prostate cancer. Prostate. 2012 Apr;72(5):487-98. doi: 10.1002/pros.21449. Epub 2011 Jul 11. PubMed PMID: 21748755; PubMed Central PMCID: PMC3248613.

Zabransky DJ, Nirschl CJ, Durham NM, Park BV, Ceccato CM, Bruno TC, Tam AJ, Getnet D, Drake CG. Phenotypic and functional properties of Helios+ regulatory T cells. PLoS One. 2012;7(3):e34547. doi: 10.1371/journal.pone.0034547. Epub 2012 Mar 30. PubMed PMID: 22479644; PubMed Central PMCID: PMC3316700.

Hallinger K, **Zabransky D,** Kazmer K, Cristol D. (2010). Birdsong Differs between Mercury-polluted and Reference Sites *The Auk, 127* (1), 156-161 DOI: 10.1525/auk.2009.09058

Narasimha R, Aganj I, Bennett AE, Borgnia MJ, **Zabransky D**, Sapiro G, McLaughlin SW, Milne JL, Subramaniam S. Evaluation of denoising algorithms for biological electron tomography. J Struct Biol. 2008 Oct;164(1):7-17. doi: 10.1016/j.jsb.2008.04.006. Epub 2008 Apr 22. PubMed PMID: 18585059; PubMed Central PMCID: PMC2435207.

Sougrat R, Bartesaghi A, Lifson JD, Bennett AE, Bess JW, **Zabransky DJ**, Subramaniam S. Electron tomography of the contact between T cells and SIV/HIV-1: implications for viral entry. PLoS Pathog. 2007 May 4;3(5):e63. PubMed PMID: 17480119; PubMed Central PMCID: PMC1864992.

Conference Presentations/Posters

4th International Conference on Electron Tomography (2006)

"3D imaging of the contact between T-lymphocytes and the AIDS virus." Sougrat R., **Zabransky D.**, Bartesaghi A., Bennett A., Wu X. and Subramaniam S.

2007 NIH Summer Student Poster Day, Bethesda, MD

"Electron Tomography of Viruses and Cells: 3D Imaging of the AIDS Virus/Mapping the HIV Envelope"

National Cancer Institute Student Research Day 2007 Talk

"Studying HIV Using Automated 3D Volume Extraction from Tomographic Data"